Characterization of a degradable polar hydrophobic ionic polyurethane using a monocyte/ endothelial cell co-culture (*in vitro*) and a subcutaneous implant mouse model (*in vivo*)

Sarah McDonald

This thesis is submitted as a partial fulfillment of the M.Sc. program in the department of Biochemistry, Microbiology and Immunology

ABSTRACT

A degradable/polar/hydrophobic/ionic (D-PHI) polyurethane with properties intended to promote tissue regeneration in a small diameter peripheral artery vascular graft was evaluated for cell biocompatibility and growth. Films were cast in polypropylene 96 well plates for monocyte/endothelial cell (EC) co-culture *in vitro* studies and porous scaffold discs were implanted in an *in vivo* subcutaneous mouse model. After 7 days in culture the co-culture demonstrated cell adhesion and growth, low esterase activity (a measure of degradative potential and cell activation), no detectable release of pro-inflammatory cytokine (tumour necrosis factor -α) but measurable anti-inflammatory interleukin (IL)-10. The EC and the co-culture expressed the EC biomarker CD31, whereas the monocyte monoculture did not.

Cytokine array analysis of the *in vivo* characterization of D-PH supported an anti-inflammatory phenotype of cells at the site of the implant. Levels of IL-6 significantly decreased over time while IL-10 was significantly higher at 6 weeks post implant. TNF-α levels did not change significantly from 24 hours onwards, however the trend was towards lesser amounts following the initial time point. Histological analysis of the explanted scaffolds showed excellent tissue ingrowth and vascularization. A live/dead stain showed that the cells infiltrating the scaffolds were viable. Both the *in vitro* and *in vivo* results of this thesis indicate that D-PHI is a good candidate material for tissue engineering a peripheral artery vascular graft.

TABLE OF CONTENTS

ABSTRACT……I

TABLE OF CONTENTS……II

LIST OF FIGURES……...IV

LIST OF ABBREVIATIONS……...V-VI

ACKNOWLEDGEMENTS……VII

LIST OF CONTRIBUTIONS……VIII

1.0 INTRODUCTION……....1-20

2.0 HYPOTHESIS……..…21

3.0 OBJECTIVE……21

4.0 MATERIALS AND METHODS……...22-33

5.0 RESULTS……...34-62

6.0 DISCUSSION……63-72

7.0 CONCLUSION……73

8.0 FUTURE OF PROJECT ……..……74

APPENDIX……..…75-78

REFERENCES…….....……..79-85

LIST OF FIGURES

Figure 1: Scanning electron microscopy (SEM) of the EC, MC and the co-culture at two weeks.

Figure 2: Phase contrast images of the EC, MC and the co-culture. MCs (A), endothelial cells (B), and co-culture (C) cultured on D-PHI for 1 week

Figure 3: DNA content of lysate obtained from MC, EC and co-culture

Figure 4: MTT assay for cellular proliferation

Figure 5: Assay of growth of EC, MC and the co-culture on D-PHI

Figure 6: Esterase activity of EC, MC and the co-culture on D-PHI and TCPS

Figure 7: Immunoblotting analysis of CD31 expression in the EC, MC and the co-culture using human coronary artery endothelial cells.

Figure 8: Cytokine analysis of conditioned media of the EC, MC and the co-culture on D-PHI by ELISA after two weeks.

Figure 9: Images of the scaffold in a subcutaneous implant in the mouse.

Figure 10: SEM of an explanted scaffold following a 2 week subcutaneous implant period in the mouse

Figure 11: Histological assessment of explanted scaffolds for cell viability and tissue in growth after 1 week

Figure 12: Total protein present in lysates from explanted scaffolds at 24 hours, 1, 2, 4, and 6 weeks from a subcutaneous mouse implant model

Figure 13: Total DNA present in lysates from explanted scaffolds at 24 hours, 1, 2, 4, and 6 weeks from a subcutaneous mouse implant model

Figure 14: Cytokine antibody array of proteins on scaffolds explanted after 7 days compared to normal mouse plasma

Figure 15: Cytokine antibody array of proteins from explanted scaffolds. Levels of MCP-5 and MCP-1 at 1, 2, 4 and 6 weeks normalized to internal controls and then calculated as a ratio to 24 hours for each cytokine.

Figure 16: Cytokine antibody array of proteins from explanted scaffolds. Levels of IL-12p40p70 at 1,2,4 and 6 weeks normalized to internal controls and then calculated as a ratio to 24 hours.

Figure 17: Cytokine antibody array of proteins from explanted scaffolds. Levels of GM-CSF at 1,2,4 and 6 weeks normalized to internal controls and then calculated as a ratio to 24 hours

Figure 18: Cytokine antibody array of proteins from explanted scaffolds. Levels of IL-6 at 1,2,4 and 6 weeks normalized to internal controls and then calculated as a ratio to 24 hours.

Figure 19: Cytokine antibody array of proteins from explanted scaffolds. Levels of RANTES at 1,2,4 and 6 weeks normalized to internal controls and then calculated as a ratio to 24 hours.

Figure 20: Cytokine antibody array of proteins from explanted scaffolds. Levels of TNF-α and sTNF-RI at 1,2,4 and 6 weeks normalized to internal controls and then calculated as a ratio to 24 hours for each cytokine

Figure 21: Cytokine antibody array of proteins from explanted scaffolds. Levels of IL-10 and IL-13 at 1,2,4 and 6 weeks normalized to internal controls and then calculated as a ratio to 24 hours for each cytokine.

Figure 22: Cytokine antibody array of proteins from explanted scaffolds. Stacked bar graph showing relative levels of TNF-α and IL-10 at 6 weeks normalized to internal controls and then calculated as a ratio to 24 hours for each cytokine.

LIST OF ABBREVIATIONS

Acronym	Definition
BPO	benzoyl peroxide
BSA	bovine serum albumin
CFDA-SE	carboxylfluorescein diacetate, succinimidyl ester
D-PHI	degradable polar/hydrophobic/ionic polyurethane
DVO	divinyl oligomer
EBM-2	endothelial basal medium-2
EC	endothelial cell
ECM	extracellular matrix
EDTA	ethylene diaminetetraacetic acid
ELISA	enzyme linked immunosorbant assay
FBS	fetal bovine serum
GAPDH	glyceraldehyde 3-phosphate dehydrogenase
GCSF	granulocyte colony stimulatory factor
HAEC	human aortic endothelial cells
HCAEC	human coronary endothelial cells
HEMA	2-hydroxyethyl methacrylate
HRP	horseradish peroxidase
IL-10	interleukin-10
IL-12p40p70	interleukin-12 p40p70
IL-13	interleukin-13
IL-1β	interleukin-1β
IL-3	interleukin-3
IL-6	interleukin-6
LDI	lysine diisocyanate
LDL	low density lipoprotein
LPS	lipopolysaccharide
MAA	methacrylic acid
MCP-1	monocyte chemotactic protein-1
MCP-5	monocyte chemotactic protein-5
MDM	monocyte derived macrophage
MMA	methyl methacrylate
MTT	3-(4,5-dimethylthiazol-2-yl)-2,5-diphenyltetrazolium bromide
NO	nitric oxide
OCT	optimal cutting temperature
PAD	peripheral arterial disease
PBS	phosphate buffered saline
PCL	polycaprolactone
PCN	poly(hexamethylene carbonate) diol
PI	propidium iodide
PLGA	poly(lactic-co-glycolic acid)
PNB	p-nitrophenylbutyrate

RANTES	regulated on activation normal T cell expressed and secreted
SDS-PAGE	sodium dodecyl sulfate polyacrylamide gel electrophoresis
SEM	scanning electron microscopy
sTNF-R1	soluble tumor necrosis factor receptor 1
TCPS	tissue culture polystyrene
TNF-α	tumor necrosis factor-α
VSMC	vascular smooth muscle cells
WST	water soluble tetrazolium

ACKNOWLEDGEMENTS

First and foremost I would like to thank my supervisor Dr. Rosalind Labow for her continuous support. She has consistently provided guidance and insight with both my experiments and my writing for which I am extremely grateful.

I would also like to thank Kelsey Santerre for her help over the summer of 2010. Without her assistance it would have been a challenge to complete all of my lab work as well as finishing my thesis.

Finally, I would like to thank Drew Kuraitis and Branka Vulesevic for their technical assistance in the *in vivo* studies and Soroor Sharifpoor for D-PHI synthesis. A special thanks to Loren Matheson for her assistance and advice with Westerns and histology and to Joanne McBane for SEM analysis and for preparing all the scaffolds and films.

This work was funded by a Collaborate Health Research Program Grant (CHRP #337246). Sarah McDonald was funded by an Ontario Graduate Scholarship, Loren Matheson by a Canadian Arthritis Network post-doctoral fellowship, Joanne McBane by a Heart and Stroke Foundation Fellowship (Focus on Stroke VII) and Drew Kuraitis by a Heart and Stroke Foundation Ontario Master's Studentship Award.

LIST OF CONTRIBUTIONS

Loren Matheson: histological analysis and production of images as well as Western for CD31 in Figure 7

Branka Vulsevic: taught surgical technique for mouse implants and scaffold preparation for histological analysis

DrewKuraitis: suggested cytokine array analysis approach and assisted with data analysis for Figure 16

Joanne McBane: performed microscopy for all SEM images and prepared all the films and scaffolds

Soroor Sharifpoor: synthesized-D-PHI

1.0 INTRODUCTION

1.1 RATIONALE

The difficulties in obtaining an autologous vessel or a synthetic substitute less than 6mm in diameter for vascular bypass surgery remain significant while the number of patients with peripheral arterial diseases (PAD) is increasing [1]. For this reason a degradable polar/hydrophobic/ionic (D-PHI) block polyurethane has been synthesized which thus far has demonstrated promising properties for vascular graft tissue engineering [2]. The long-term goal is to use this material to create a tubular scaffold and then graft a patient's autologous cells within the structure for vessel replacement. It is hypothesized that when monocytes (MC)s are recruited in the innate immune response to the graft they will initially aid in the appropriate cell recruitment and then transition to a wound healing phenotype and function in the process of tissue regeneration of a blood vessel [3].

1.2 PERIPHERAL VASCULAR DISEASE

PAD is defined as obstruction of blood flow into an arterial tree excluding the intracranial or coronary circulations [4]. It is most often a manifestation of systemic atherosclerosis resulting in an increased risk of myocardial infarction and stroke [5]. While PAD may be asymptomatic in its early stages, as the disease progresses and

obstruction of blood flow increases it will result in significant impairment in an individual's ability to carry out daily activities and their overall quality of life. Like coronary artery disease, the pathophysiology of PAD results largely from stenosis of the arteries and atherothrombosis [6]. Ultimately, this leads to resistance in the peripheral vascular system leading to decreased oxygen delivery to the tissues that worsens with physical activity. While ischemia resulting from a partially or completely occluded vessel may be debilitating in terms of activity, ulceration and eventual limb loss may result if the disease is sufficiently severe [6].

Disease management for patients suffering from PAD will vary depending on the progression of the disease. Initially, life style modifications such as the cessation of smoking, increased physical activity, aggressive management of diabetes, reduction in blood pressure if necessary, and regulation of high (low density lipoprotein) LDL levels should be considered [5]. Pharmacological interventions include antiplatelet therapy such as aspirin or clopidogrel, which was shown in a meta-analysis of 42 trials involving patients with PAD to significantly reduce vascular events by 22% [7]. Surgical interventions are often required for more severe cases and involve revascularization procedures using stents and bypass grafts [5]. In approximately 5% of patients with severe limb ischemia there are indications for amputation, which include life-threatening infections or advanced tissue necrosis [8]. The loss of a limb results in severe disability and a poor prognosis as there is a 30% to 40% mortality rate in the following 24 months [4].

In the United States approximately 500,000 coronary artery and 100,000 upper and lower limb bypasses are performed annually due to PAD and myocardial infarctions [9]. Unfortunately, in patients for whom bypass surgery is a viable option, the availability of small caliber vessels (less then 6mm) required for surgery is often limited. Such patients include diabetics and the elderly who likely have a decrease in perfusion to their peripheries that worsens with PAD, and therefore do not have autologous vessels available for bypass surgery. The use of a peripheral vascular graft for the purposes of tissue engineering a blood vessel would provide another much needed treatment option.

1.2 VASCULAR GRAFTS

To date, the search for a design to produce ready-made small diameter vessels has eluded researchers. Therefore, along with the limited supply of autologous vessels in a patient, the surgeon does not have access to an off-the-shelf by-pass graft for a small diameter vessel. As such, the field of small caliber vessel tissue engineering is an area of intense research [10], [11] and remains a promising strategy through which the creation of a small diameter vascular graft may be achieved. Variable materials and regenerative techniques have been explored yet a usable product has eluded researchers [12]. Most approaches to graft development have been hindered by poor levels of remodeling, thrombosis, inadequate mechanical properties, or the absence of a proper vasomotor response [13]

A structural scaffold, vascular cells, and a nurturing environment are all required

in order to utilize tissue engineering for revascularization [10]. In order for such a scaffold to be successful, it must possess suitable mechanical properties while allowing for the regulated proliferation of vascular smooth muscle cells (VSMC)s and endothelial cells (EC)s which will ultimately comprise the new vessel [14]**.** The final scaffold product should provide a three-dimensional structure on which isolated cells can adhere and proliferate to eventually form a functional blood vessel [10], [15]. Finally, gradual degradation of the scaffold should occur following the formation of the vessel tissue [10]. Synthetic biodegradable polymers provide a promising alternative as one can control the mechanical properties and the dimensions of the material while designing the graft [2].

For a vessel to function optimally it must have a tunica intima comprised of a functional endothelium such that the ECs form a sheet which is aligned in parallel to the flow of blood through the lumen of the vessel and is not predisposed to thrombogenicity. After the EC layer, the tunica media must comprise the connective tissue and VSMC layer of the middle portion of the vessel. These cells should be oriented in a perpendicular fashion such that they provide elasticity and contractibility of the vessel. Finally, the outermost portion of the vessel is the tunica adventia which is comprised of fibroblasts and connective tissue that help to hold the vessel together. It becomes obvious that designing a compliant graft from a scaffold that is carefully engineered to allow for such controlled and intricate cellular proliferation produces many challenges.

There are essentially two options when designing a scaffold for vessel tissue engineering and they include the use of a natural or a synthetic material. Natural

scaffolds may take the form of decellularized vessels [16], animal ureters [17], or human umbilical veins [18]. In order to prepare such a scaffold host antigens must be removed so that a vascular extracellular matrix in the form of a tube remains and tissue rejection does not take place [19]. Another option for the construction of a natural scaffold is the use of extracellular matrix-based scaffolds. These hydrogels from collagen or elastin allow for the easy incorporation of growth factors to allow the delivery of various angiogenic factors [20]. Despite the fact that this system is able to induce and support cell ingrowth and direct an appropriate cell phenotype, the structure of the vessel does not have the proper mechanical properties and is unable to maintain its form. For this reason additional support is required. The final option for a natural based scaffold is to use sheet based vessel engineering which involves rolling a sheet of autologous fibroblasts that are able to synthesize extracellular matrix into a tube, a technique used for the research conducted by L'Heureux *et al* [21]. However, due to the extensive time for tissue culture required and the incomplete cellular composition of the vessel which has no vascular smooth muscle cells, this option is often seen as less than feasible [21], [22].

Synthetic scaffolds provide an alternative to natural scaffolds which allow many problems to be avoided. Synthetic scaffolds can be designed to have adequate mechanical properties to function *in vivo* as well as being re-cellularized more rapidly. These cells must be able to grow into the scaffold structure which is accomplished by creating pores in the material while still maintaining sufficient mechanical strength. Void fraction and pore size are important aspects to consider which will affect cell ingrowth as

the cells must not only receive adequate nutrients, they must also be able to interact with each other such that proper tissue formation can take place [23]. Eventually the goal is to have a functioning vessel with regenerated tissue while the scaffold material gradually degrades.

In a review by Lian Xue [24], they discussed the numerous materials and methods involved in designing a synthetic vascular scaffold. Originally grafts were constructed from Dacron (polyethylene terephthalate) and Teflon (expanded polytetrofluoroethylene), however neither material can be used to produce a successful graft smaller than six millimeters. Dacron was first used as an implanted vascular graft in 1957 and today is clinically available in either woven or knitted forms. It is stable and may persist for more than ten years after being implanted, however, as the size of the graft decreases, so does the patency. Once the graft has been implanted protein adsorption takes place on the surface of the material, then platelets adhere and inflammatory cells infiltrate followed by EC and smooth muscle cell infiltration. The fibrin, platelets and blood cells build up during these first few days and eventually stabilize after six to eighteen months. When examining the grafts histologically, one observes a compact, acellular fibrin layer on the surface in contact with blood and densely packed foreign body giant cells in the space between the capsule which forms around the graft and the graft itself. Meanwhile, Teflon provides a biostable graft material which does not degrade and provides an electronegative surface which decreases the reaction with blood. However, the host response is similar to that of Dacron, and years after implantation, there is still a lack of

luminal surface cellular coverage. Overall, both of these materials display similar rates of patency in all locations. [24]

The current availability of materials with greater elasticity and degradability has broadened the number of possibilities for graft development. These include materials such as polycaprolactone (PCL) and poly (lactic-co-glycolic acid) (PLGA) which are typically used in drug delivery systems but also have potential for vessel tissue engineering since they degrade [25], [26]. The addition of extracellular matrix (ECM) protein coating to these materials potentially aids in cell adhesion as well. Hybrid polymers are another possibility which use combinations of synthetic and natural materials to produce a final product with optimal strength and degradability.

1.3 INNATE IMMUNE RESPONSE

When designing a vascular graft for tissue engineering there are three main factors which one must take into account. The interaction between the material and the cells will affect the levels of toxicity, the elicited immune response invoked by the material, and the differentiation of the cells which is induced on the surface of the scaffold. Another aspect which must be taken into account is the mechanical properties of the scaffold such as its porosity and mechanical strength as well as its durability. Finally, the interaction of the scaffold within its environment such as protein adsorption and the degree of swelling will affect the functioning of the final product. These factors are affected by the innate immune response which will determine how the body responds

to the material and the degree to which cells are able to proliferate and develop the proper phenotype for vessel growth as well as the degradation of the material, another necessary feature of a successful vascular graft.

Although the use of polymers from natural sources such as collagen may not be as likely to elicit a strong immune response against the material, they pose their own set of problems such as lack of durability, decreased availability, and risk of infection. Synthetic materials such as polylactides, polyglycolides and their copolymers form degradation products that make the surrounding environment acidic thus eliciting an inflammatory response and decreasing the biocompatibility of the material [27]. The goal in the development of a synthetic material is to design a material that elicits an immune response which creates a supportive environment, actually directing tissue repair such that the cells assume the functional phenotypes of vascular tissue [27].

A review written by Anderson *et al* provides an excellent description of the foreign body reaction to biomaterials which is initiated following implantation and the modulating factors of this response [28]. Following the implantation of a device numerous host reactions take place including blood-material interactions, matrix formation, acute and chronic inflammation, granulation tissue development, foreign body reaction, and fibrous capsule development [29], [30]. Following the initial adsorption of proteins on the biomaterial surface a provisional matrix is formed from the clotting cascade which is also initiated. This initial covering sets the environment for wound healing and tissue regeneration so it is important that the cytokines and growth factors

present are appropriate for this process. This will affect the response from neutrophils that will be recruited to the area to begin the phase of acute inflammation. Chronic inflammation usually follows after approximately one week and is characterized by the presence of mononuclear cells such as monocytes and the initiation of the foreign body reaction involving monocytes, macrophages, and foreign body giant cells. Once the inflammatory response subsides, usually after no more than three weeks, granulation tissue forms which involves the recruitment of fibroblasts and ultimately the formation of a fibrous capsule. Underneath this capsule the foreign body reaction continues on the surface of the material. [28]

The goal is to design a material that may at first recruit inflammatory cells but will subsequently allow these cells to transition to a wound healing phenotype to direct tissue repair.

1.4 MONOCYTES

Following the implantation of a material into the body, a wound healing or foreign body response may be initiated as determined by the compatibility of the material. MCs and monocyte-derived macrophages (MDM)s play a central role in determining the immune response to the implant by adopting an inflammatory or wound-healing phenotype, characterized by the cytokines secreted into their local cellular environment. Since the chemical structure of the material surface has been shown to

influence the eventual phenotype of the MDM, the components of the graft material are of integral importance in determining the success of the graft itself [13].

Despite the vast amount of research being conducted in the field of vascular graft generation the importance of the components of the material and the ultimate effect from an elicited immune response tend to be overlooked. Neutrophils, MCs and MDM play a critical role in controlling the overall process and success of tissue integration [31], [32], [33].

Following the activation of an MDM, a vast number of different inflammatory mediators are released into the local environment [28]. These mediators serve two functions, the first being to phagocytose the biomaterial on which they are located, and the second to direct wound healing and the inflammatory response. It has been shown that the cytokines released by MDM vary with material surface chemistry as well as the proteins which are adsorbed following implantation [28], [34]. Thus MDM activation can be modified by the chemical structure of the surface as well as its topography [28].

The phenotype adopted by the MDM will ultimately affect the cytokines which are released into the local environment and is referred to as M1 and M2. The classically activated MDM, M1, has a pro-inflammatory phenotype and thus releases pro-inflammatory cytokines and inhibits those which are anti-inflammatory. This type of MDM is typically activated by microbial products such as lipopolysaccharide (LPS) [28], [35] and secretes nitric oxide (NO). It is associated with tissue destruction, killing of intracellular parasites, and tumor resistance [36]. The second type of MDM

phenotype, M2, involves anti-inflammatory, wound healing cytokine secretion. M2 polarization is associated with tissue remodeling and angiogenesis, parasite encapsulation, and tumor promotion [36]. Obviously, it is the latter which we wish to induce by carefully modifying the chemical components of a material intended for vascular graft synthesis. Using these signaling pathways the MDM recruit blood derived stem cells [37], and depending on the stem cells recruited, the final phenotype of the VSMCs and ECs may be affected.

1.5 ENDOTHELIAL CELLS

The first step which must be taken care of when producing a functioning vessel of less than five millimeters diameter with a synthetic material is ensuring that thrombosis or vessel occlusion does not occur. It is also important to ensure that the proper phenotype is adopted by the EC as there is a growing body of knowledge with regards to the heterogeneity of ECs that line arteries and veins [38], [39].

Circulating endothelial progenitor cells have been shown to be capable of differentiating into the ECs necessary to line the graft [40]. An important issue that may arise is the quality of these cells in patients whose vessels are already diseased. The function and number of these cells have been shown to be reduced under such circumstances [41] but could possibly be improved upon in quality [42].

It is also possible to culture both EC and VSMCs by using bone marrow mesenchymal stem cells which are autologous in origin, highly proliferative, and have the

potential to differentiate into vascular phenotypes which have been shown to be influenced by growth factors released at the site of vessel injury [43]. In fact, it has been demonstrated that injured endothelium and media in arteries are repaired by stem cell populations derived from bone marrow further indicating the benefit of using such a population of cells for seeding a graft [44].

Intact, functioning endothelium is integral to achieving a functional vessel. In fact, *in vivo,* endothelial dysfunction is considered one of the first steps toward developing arteriosclerosis [45]. Relaxation of the underlying smooth muscle is initiated by the endothelium through the release of NO amongst other endothelium derived hyperpolarizing factors [45]. Acetylcholine, physical forces, circulating hormones, platelet products, and prostaglandins can all initiate the NO response which acts as an important mediator in the vasodilatory mechanism. By preventing abnormal constriction of the arteries and inhibiting the aggregation of platelets it has an important role in protection against the inflammatory response that leads to atherosclerosis and occlusion of grafts [45]. For this reason achieving a confluent layer of regulated endothelial cells in the lumen of a graft is extremely important and must be assessed through *in vitro* and *in vivo* experiments.

1.6 **VASCULAR SMOOTH MUSCLE CELLS**

While VSMCs are not a central focus of this thesis, they are very important in the development of a vascular graft. When VSMCs are cultured *in vitro* they can show

varying phenotypes which may be useful when designing a graft, but also pose several challenges. Essentially this cell type may be of the proliferative synthetic variety or display properties of the quiescent contractile phenotype. The challenge in designing an artificial vessel is to harness the properties of each phenotype at different points during the process of tissue regeneration. In a healthy vessel cells are contractile and do not proliferate. However, the synthetic phenotype is found during diseased states such as atherosclerosis and is also elicited when these cells are cultured *in vitro*. When designing a vessel it is necessary to harness the properties of the synthetic phenotype in order to populate the graft and allow for tissue formation [46]. Once this has been accomplished it is then necessary to induce the contractile phenotype which allows a functional vessel to contract and dilate and is apparent by the presence of markers such as smooth muscle α-actin, calponin, and myosin heavy chain. [46].

VSMCs and ECs are the main components in a vessel wall and the interactions between the two cell types are integral in the control of normal growth and function [47]. In normal vessels VSMCs are surrounded by basement membranes and the lumen of the vessel is lined by ECs which prevent the proliferation of VSMCs, which when uncontrolled is a key aspect of vascular disease [48].

1.7 **MONOCYTES & ENDOTHELIAL CELLS**

As stated, ECs play a central role in the formation of a functional blood vessel and their phenotype and proliferation are, in part, regulated by MCs [49]. While previous

research indicates that a completely non-reactive material for graft construction is unlikely to be found, proper endothelialization of the lumen of a graft would greatly assist in increasing its overall patency [22]. The generation of a smooth EC surface, producing natural biochemicals, would produce an intra-lumen environment similar to a native vessel and decrease the risk of a thrombogenic event [50]. While endothelialization is an important step in blood vessel growth, proliferation of both ECs and VSMCs must be regulated in order to prevent hyperproliferation which could lead to intimal hyperplasia.

The proliferation of ECs is a tightly regulated process that is controlled by a diverse range of growth inducing and inhibiting factors which ultimately results in an intact endothelial monolayer in a vascular bed [24]. It has been documented that MCs are recruited to sites of vascular remodeling after angioplasty or stent implantation in atherosclerotic lesions and in tissues where ischemia is induced [15], [51], [52].

MCs have been shown to play an active role in endothelial cell proliferation as they synthesize and secrete cytokines and growth factors which aid in vessel repair [49]. Studies have shown that following rabbit femoral artery occlusion, collateral arteries that develop express adhesion molecules and have adherent MCs 12 hours following occlusion of the vessel [53]. It has also been shown that intraarterial infusion of monocyte chemoattractant protein (MCP-1) significantly increases the level of perfusion in an ischemic porcine hindlimb [54]. Therefore, a key aspect of this thesis is to examine the influence of MCs and ECs on one another in the overall process of tissue

regeneration.

1.8 INFLUENCE OF MECHANICAL FORCES

The stresses applied to ECs and VSMCs as they are proliferating are also important. While blood flow generates frictional forces on the endothelial cells, blood pressure generates cyclic circumferential stretch on the vessel wall which is of particular importance to VSMCs [55, 56]. It has been shown that within an artery, they are subjected to circumferential cyclic tensile strain of 5-10% [57]. For this reason mechanical conditioning of the cells is an important component of creating a functional vascular graft [58] and bioreactors have been developed to apply the appropriate mechanical stimuli to the cells.

Studies have indicated that VSMC-EC interactions are affected by mechanical forces with regards to migration, proliferation, and apoptosis [47]. In fact, Wang *et al* have shown that VSMC/EC co-cultures experience a down regulation in VSMC migration under shear stress, whereas in its absence migration is stimulated [47]. Other studies have shown the down regulation of the markers associated with the contractile phenotype of VSMCs under static conditions [59].

1.9 POLYURETHANES

The material of choice for the research described in this thesis is D-PHI, a polyurethane specifically modified for use in vascular tissue engineering. Polyurethanes,

generally, are versatile materials that have been used in the body for a great variety of medical devices for over thirty years [60], thereby demonstrating the benefits of their use in the field of tissue engineering. They have been important in the development of a variety of medical devices ranging from use in catheters to pacemaker leads. They are both mechanically stable and elastomeric as well as providing an option for structural tailoring with regards to mechanical strength and degradation. There are numerous papers describing the use of these materials and the possible modifications to which they may be subjected in order to optimize their use in the field of medicine [60].

Polyurethanes are constructed by polymerizing, in the presence of a catalyst, a monomer containing at least two hydroxyl groups with one containing at least two isocyanate functional groups, referred to as a diisocyanate. This produces a polymer linked by urethane groups and allows for a wide variety of final products. These polymers exemplify properties such as durability, fatigue resistance when under tensile forces, and a propensity for the promotion of healing [61]. Another benefit to using polyurethanes is that they can be specifically surface modified by adjusting the hydrophilic/hydrophobic balance of the monomer or by attaching biologically active species [61].

1.10 BACKGROUND

D-PHI is a polyurethane specifically chemically modified to promote cell attachment along with promoting a MC wound healing phenotype that will direct the formation of a functional vessel. A significant amount of work has already been conducted on D-PHI synthesized with specific attention to its physical and chemical properties for peripheral vascular graft synthesis. When synthesizing this material the end goal was to create a surface that would minimize the inflammatory nature of MCs and provide similar mechanical properties to a native vessel. Another important aspect that was taken into consideration when developing this material was the ionic nature of the surface. Different monomers were used to produce a final product with balanced hydrophilic and hydrophobic character, with an end goal of optimizing cell adhesion and proliferation. While it has been shown that cells adhere preferentially to hydrophilic surfaces, excessive hydrophilicity tends to decrease EC proliferation and adhesion.

Another important characteristic of D-PHI is that while the material can be cast into a solid form, it can also be constructed into a porous scaffold to allow for cell infiltration. This scaffold possesses high porosity (~80%) and pore interconnectivity for cell proliferation and low cytotoxicity. [57]

Recent studies showed that when monocytes were cultured on films and compared to scaffolds, it was found that D-PHI in scaffold form appeared less activating. D-PHI was synthesized by first producing a divinyl oligomer (DVO) using lysine-diisocyanate (LDI), poly(hexamethylene carbonate)diol (PCN), and 2-hydroxyethyl methacrylate (HEMA) in a 2.00:1.00:2.01 stoichiometric molar ratio. This lysine based DVO was then reacted in a 1:5:15 ratio of DVO, methacrylic acid (MAA), and methyl

methacrylate (MMA) respectively [2]. Each segment of the polyurethane was carefully selected in order to improve the mechanical properties and the degradation products of the polymer. The PCN segment provides increased tensile strength and is more susceptible to hydrolytic degradation, producing carbon dioxide and hexane diol which will not initiate an immune response. LDI provides a diisocyanate which degrades to form lysine, a normally occurring amino acid. HEMA was selected as it provides the ability for cross-linking as well as an ester group which improves hydrolytic degradation [2].

Hydrolytic degradation makes the scaffold susceptible to esterase activity, improving the overall rate at which it will degrade. As well as inducing oxidative degradation, MDM have been shown to synthesize and secrete different amounts of cholesterol esterase and monocyte specific esterase when cultured on PCNUs with differing surface chemistries [62]. Overall, cholesterol esterase is the enzyme with the potential for causing the greatest amounts of biodegradation of PUs, thus confirming that macrophages may play an important role in the degradability of D-PHI [63].

The concept of using a biomaterial that is susceptible to degradation is integral when designing a medical device intended as a substitute to provide a specific physical/mechanical function for a given amount of time. To date biodegradable polymers used in clinical applications consist of a macromolecule containing hydrolytically cleavable backbone bonds making them susceptible to hydrolytic degradation. When an MDM is in contact with a surface that is too large to engulf it will begin a process referred to as frustrated phagocytosis leading to the release of reactive oxygen species and hydrolytic enzymes [63]. Following the formation of foreign body

giant cells composed of MDMs which have fused together, secretion is increased. Since the surface of the material will play a role in the maturation and activation pathway of MCs, secretory products such as esterase may be viewed as a sign of cellular activation and directly influenced by the surface on which the cell resides [63]. Therefore, the biocompatibility of the material will influence the nature of the inflammatory cells on its surface, and the biostability of the material, which is inherent in its chemical composition, will determine the overall rate at which a device will degrade [64].

Studies thus far have confirmed the suitability of D-PHI for scaffold synthesis in order to tissue engineer a vascular graft. Not only did D-PHI maintain cell attachment, it also enhanced the transition of the MDM to a wound healing phenotype when examining relative levels of pro-inflammatory and anti-inflammatory cytokines [3]. **S**ignificantly more interleukin 10 (IL-10) was released over time than interleukin 1β (IL-1β) and tumor necrosis factor α (TNF-α) when compared with cells cultured on tissue culture polystyrene (TCPS) [3].

In addition, studies comparing films to scaffolds showed that MCs differentiated to a lower inflammatory state on the scaffolds [65]. While collagen coating improved the amount of DNA found on TCPS, uncoated D-PHI also had significantly more DNA than uncoated TCPS as well as significantly less esterase activity suggesting that its surface chemistry may resemble ECM proteins. When VSMCs were seeded on D-PHI and placed under cyclical mechanical strain they displayed a more favorable phenotype for vessel construction [57]. Moreover, when co-cultured with MCs, significantly more VSMC penetrated the scaffold [66].

In this thesis the effect on co-culturing ECs with MCs was investigated on D-PHI films *in vitro,* while *in vivo* experiments examined the inflammatory response evoked by the material when D-PHI scaffolds were implanted in a subcutaneous mouse model.

2.0 HYPOTHESIS

A degradable polar hydrophobic ionic polyurethane synthesized with ECM-like properties will shift MCs towards an M2 MDM phenotype such that a local environment conducive to tissue repair is created, allowing for the controlled proliferation of functional EC on the graft material.

3.0 OBJECTIVE

To characterize a novel degradable polar hydrophobic ionic polyurethane material (D-PHI) *in vitro* with an EC/MC co-culture and *in vivo* with a mouse subcutaneous implant model

3.1

To assess growth, esterase activity and cytokine production in an EC/MC co culture on D-PHI films *in vitro*.

3.2

To assess the inflammatory response activated by D-PHI in scaffold form when implanted *in vivo* in a mouse subcutaneous model using cytokine antibody arrays and histological techniques to examine tissue ingrowth.

4.0 Materials and Methods

Unless specified otherwise all reagents were purchased from Sigma–Aldrich, Oakville, ON, Canada.

Polymer synthesis –films and scaffolds

All polymer synthesis was completed according to the procedure of Sharifpoor *et al* [2]. Briefly, a DVO was synthesized by reacting hydroxyethylmethacrylate, polyhexamethylene carbonate diol and LDI in a 2:1:2 ratio in dimethylacetamide with dibutylin dilaurate as a catalyst. The D-PHI material was made by mixing DVO (acts as a cross-linker) with MAA and MMA in a ratio of 1:5:15 respectively, in the presence of a benzoyl peroxide (BPO) initiator (0.0015 mol/mol vinyl group) and left to mix for 18-24h. In order to make the films, the mixture was cast in a 96-well polypropylene plate and cured at 110°C for 24h in a nitrogen-filled oven. The films were then stored in the dark and were soaked in 70% ethanol for 3-5 hours prior to use. Following this procedure, the films were transferred to a 96-well tissue culture polystyrene plate and hydrated overnight in phosphate buffered saline (PBS) buffer with 4% penicillin/streptomycin prior to seeding with ECs.

The same polymerization reaction was used to create the scaffolds (70% porous) [2]. After the addition of BPO initiator, the resulting blend was allowed to mix for a minimum of 12 hours (room temperature, light protected) prior to the addition of $NaHCO_3$ particles (65wt% relative to resin (95wt% of particles are in the range of 105-420 μm)). Following an additional 12 hours of mixing (room temperature, light

protected) the final paste was loaded into Teflon molds (6mm diameter, 2mm thick) and cured at 110°C for 24 hours. Upon the completion of the curing process, the disk-shaped scaffolds were subjected to a 14-day salt leaching process in distilled and deionized water.

Isolation of MCs

Human MCs were isolated using Histopaque 1077 and differential centrifugation from 30 mL of blood donated from healthy volunteers and collected into ethylenediaminetetraacetic acid (EDTA)-containing Vacutainers (Becton Dickenson, Toronto, Canada) with approval of the Ottawa Hospital Research Ethics Board, Ottawa, Canada (protocol number UOHI 2005979-01H valid until Feb. 18, 2011) as described in detail previously by Matheson *et al* [63]. The blood was layered onto 20 mL of Histopaque 1077 in a 50 mL polypropylene centrifuge tube (Falcon 2098). Centrifugation took place at 800 x g (2000rpm, Model RT6000B) with the brakes off. The plasma layer was removed and the layer containing MCs was transferred to a new 50 mL Falcon tube where it was washed 5 times using 30 mL of wash buffer (282 mL RPMI, 3 mL fetal bovine serum (FBS), 15 mL 6.5% EDTA) followed by centrifugation at 1400 rpm (450 x g) in the RT6000B with the brakes on for 10 minutes/wash after re-suspending the pellet following each wash. After the final wash, the pellet was re-suspended in 10% FBS media and counted in the automated Vicell^{TM} Cell Viability Analyzer/Cell Counter (Beckman Coulter; Miami, FL).

Co-culture of endothelial cells and monocytes

Human coronary artery ECs (HCAEC) (Lonza) were cultured in supplemented Clonetics endothelial cell basal medium (EBM-2) (Lonza) (supplemented with fetal bovine serum, ascorbic acid, rHuman fibroblast growth factor-B, recombinant human epidermal growth factor, recombinant long R insulin-like growth factor-1, hydrocortisone, vascular endothelial growth factor, gentamicin sulfate amphotericin-B) in a 25 mL tissue culture flask until confluent (from 3-5 days). All ECs used for experiments were between passages 2 and 4. Co-cultures were established by ECs seeded and cultured alone for 24h, after which MCs (isolated as described above) were added in a 3:1 ratio of MCs:ECs (30 000:10 000) unless otherwise stated. As the surface area of the 96 well plate is approximately 28 mm^2 the seeding density is approximately 1071 MCs/mm^2 and 357 ECs/mm^2. These densities were considered appropriate as MCs are much smaller and do not replicate whereas ECs are larger and proliferative. The co-cultures and each individual cell culture (MCs and ECs alone) were then maintained with a 50:50 mixture of RPMI media and EBM-2 media. The medium was changed 2 hours after the MCs were seeded and every 48 hours onwards with 200μL of media composed of 50% of RPMI media (10% FBS, 2% penicillin/streptomycin and 0.69 mM L-glutamine in RPMI with 12.7 mM HEPES) and 50% EBM-2. Both cell types were able to survive, and the ECs were able to proliferate well in this combination of media.

Scanning electron microscopy (SEM)

Cells cultured on the D-PHI films *in vitro* and the explanted scaffolds, after two weeks *in vivo,* were fixed in 3% glutaraldehyde in PBS and then stored in PBS at 4^{o}C prior to SEM analysis as described previously [67]. They were then dehydrated with increasing concentrations of ethanol (30%, 50%, 70%, 90%, 95%, and 100% for one hour each) before critical point drying, mounting on stubs, and platinum coating. The samples were photographed using a Hitachi S 2500 Scanning Electron Microscope (Hitachi, Mito City, Japan) at an operating voltage of 10 kV.

Phase contrast microscopy

Images were obtained using an Olympus CK2 light microscope and an Infinity 2 camera.

Assay of DNA

DNA present in the cells was assayed following the preparation of cell lysate according to the procedure of Matheson et al [63]. This was accomplished using 75 µL of cold TritonX-100 buffer (0.05% TritonX-100, 10mM EDTA in PBS (0.2g/L KCL, 0.2g/L KH_2PO_4, 8.0g/L NaCl, 1.144g/L Na_2HPO_4) which was added to each well. The cells were then allowed to lyse for 1h on ice. Hoechst Dye (#33258; Amersham Biosciences, Baie d'Urfe, QC, Canada) was prepared by diluting 10 µL in 10mL of 1x TNE buffer (100mM TRIS base, 2.0M NaCl, and 10mM EDTA in ddH2O), pH 7.4, prior to addition to the lysate. 100 µL of the dye was then added to 10 µL of the lysate in a black 96-well plate (Microfluor 2 Black; VWR, Mississauga,

ON, Canada) and read against a standard DNA curve in a fluorescence microplate reader (POLARstar Galaxy, BMG Technologies; Durham, NC) using an excitation and emission wavelength of 360 nm and 460 nm respectively.

MTT Assay

The (3-(4,5-dimethylthiazol-2-yl)-2,5-diphenyltetrazolium bromide) MTT assay was carried out using a solution of Thiazolyl Blue Tetrazolium Bromide (according to the method supplied by Sigma) at a concentration of 5 mg/mL in the 50:50 media that the cells were cultured in. After removing the regular media from each well, 100 µL of the MTT solution was added to each well. The cells were then returned to the incubator where they remained for the following 4 hours. At this point, the MTT solution was removed and 100 µL of MTT solvent (0.1 N HCl) was added to each well. The wells were then scraped and mixed thoroughly in order to dissolve the formazan crystals that formed over the course of the incubation. The plate was then read in an absorbance microplate reader (POLARstar Galaxy, BMG Technologies; Durham, NC) at 570 nm.

Assay of Growth with WST

The cell proliferation reagent, water soluble tetrazolium (WST)-1 (ROCHE, Cat No. 05015944001), was used to measure cell activity and growth at 48 hours, 96 hours and 7 days (cells plated at MC:EC 30 000: 2500 in order to observe a linear growth rate of EC). 10µL of WST-1 and 90 µL of media were added to each well and left to incubate until a colour change was observed. Plates were read in a microplate reader

(Bio-Rad Model 3550-UV) at an absorbance of 450nm with the background at 690nm being subtracted. Data were normalized to absorbance (optical density (OD)/hour).

Assay of esterase activity

After 48 hours of culture, conditioned media (cell supernatant) and lysates were collected and assayed for esterase activity as described in detail previously by McBane *et al* [68]. The substrate p-nitrophenylbutyrate (PNB) was used to define a unit of activity which is equal to the release of 1nmol of p-nitrophenol (ϵ=16,300$cm^{-1}M^{-1}$) per minute at 37^{o}C at pH 7.0 at 400.6 nm over a 30 minute incubation. The activities were then normalized to 1 μg of protein.

Assay of protein content

The amount of protein in the lysate obtained from each cell culture sample was assayed using the Bradford method [69] (reagent obtained from Bio-Rad Laboratories Ltd., Mississauga, ON, Canada). Bovine serum albumin (BSA) was used to create a standard curve for which to compare the protein content of each sample.

Immunoblotting Analysis of CD31

Samples were loaded based on protein values determined using the Bradford method. As previously described [63], sodium dodecyl sulfate polyacrylamide gel electrophoresis (SDS-PAGE) gels used for immunoblotting analysis were transferred to a BioTRace nitrocellulose membrane (VWR), followed by blocking in a 5% BSA solution in TBS-Tween20. The nitrocellulose membrane was incubated with CD31

(R&D Systems) in 1:200 dilution in 1% BSA in the cold room overnight at 4°C. Blots were washed and incubated with secondary goat anti-mouse immuno-globulin G antibody conjugated to horseradish peroxidase (Pierce Chemical Co., Gilbertsville, PA) 1:2500 in 5% BSA). Protein bands were visualized with an enhanced chemiluminescence detection system (Thermo Scientific, SuperSignal West Femto) and recorded on Kodak X-ray film (Fisher Scientific).

Assay of Cytokines by ELISA

Enzyme linked immunosorbant assays (ELISA)s for TNF-α (Cat No. 88-7346-88) and IL-10 (Cat No. 88-7106-88) were carried out according to the protocol and the certificate of analysis supplied by the manufacturer (eBioscience) in each kit using cells plated at MC:EC 60 000: 20 000 to increase concentration of cytokines in the conditioned media. Costar 9018 high binding capacity plates (eBioscience) were coated with capture antibody in coating buffer overnight at 4°C. Plates were then washed and blocked with assay diluent. Standards supplied in the kit were used to create the standard curve and 100 µL of the conditioned media were placed in each well. Samples were left to incubate overnight at 4°C. Plates were washed the following day and then detection antibody was added for 1 hour followed by another series of washes. Avidin-horseradish peroxidasae (HRP) was then added for 30 minutes followed by washes and the addition of substrate solution for 15 minutes. Stop solution consisting of 2N sulfuric acid was then added before the plates were read at 450nm in a microplate reader as above.

***In vivo* surgery/scaffold preparation**

BALB/c mice (female, ~ 20g, 4-6 weeks) (Charles River, Wilmington, MA) were anaesthetized with isofluorane and 2 scaffolds/mouse were placed in subcutaneous pockets on the dorsal surface of the animal and the incision closed with sutures (7-0 silk) (approval by the Animal Care Veterinary Service Committee, University of Ottawa, Ottawa, ON, Canada, protocol HI-326 valid until August 13, 2014). Prior to the implantation, scaffolds were treated with a 70% ethanol solution overnight and then left in sterile filtered PBS containing 4% penicillin/streptomycin.

Cytokine antibody arrays were first conducted on lysates from a 1 week explant from 3 mice as well as collecting blood into EDTA vacutainers for plasma preparation from animals that did not have implanted scaffolds in order to obtain normal plasma values which acted as controls. The second set of cytokine data were acquired from fifteen mice (3 mice per time point) for a time course from 24 hours, one week, two weeks, four weeks, and 6 weeks. At the time of explantation, all scaffolds were removed and placed in cold PBS on ice.

For histological analysis, a 1 week scaffold sample was fixed in 4% paraformaldehyde for 25 minutes before being dehydrated in consecutive solutions of 15% and 30% sucrose. Following the dehydration procedure, this scaffold was sliced (Cryostat, Leica CM3050S) in 25 μm thick slices after being embedded in Optimal Cutting Temperature (OCT) compound (Tissue-Tek, Sakura). Slices were placed on Superfrost Plus White pre-cleaned 25 x 75 x 1 mm micro slides (VWR Micro Slides) prior to staining for histological analysis. Another scaffold explanted after 1 week was

fixed in 3% glutaraldehyde for SEMs and processed as described above. Scaffolds were also implanted in mice for 1 week in order to examine acute viability using a live/dead assay described in detail below.

Cytokine antibody array

RayBio mouse cytokine antibody arrays (RayBiotech, Inc. Cat# AAM-CYT-1) were utilized in order to assess which cytokines present in the explanted scaffolds as well as their relative amounts. The explanted scaffolds and normal mouse plasma were allowed to thaw and then 2 mL of cell lysis buffer (supplied with the array kit) was added to the scaffold prior to homogenization in a hand held Dounce homogenizer. Protease inhibitor was added to each sample in a ratio of 1:200. Bradford assays were performed to assess protein levels in the homogenates, and cytokine antibody membranes were incubated with 300 μg of lysate or plasma protein according to the manufacturer's protocol. Detection took place in a chemiluminescence imaging system (FluorChemHD, Alpha Innotech). The quantification of each image was carried out by AlphEaseFC software normalizing each cytokine to the positive controls included on each membrane.

For the first 1 week implant for cytokine analysis, selected cytokine values in both lysates and plasma (granulocyte colony stimulatory factor (GCSF), G macrophage (M)-CSF, interleukin (IL)-3, monocyte chemotactic protein (MCP)-1, MCP-5) were calculated as ratios to tumor necrosis (TNF)-α. For the time course analysis of cytokine production, all cytokines assessed were normalized to their values at 24 hours after normalizing all values on the arrays to an internal positive control.

Histological Analysis:

Trichrome Stains

Following the slicing using a cryostat as described above, and removal of OCT from the explanted scaffolds with PBS, Masson-trichrome staining was used to distinguish connective tissue, muscle, and collagen fibers. Briefly, the slices were placed in preheated Bouin's Solution (HT10-1) at 56°C for 15 minutes then allowed to cool in tap water at room temperature. The slides were then washed in tap water and stained in Weigert's Iron Hematoxylin Solution for 5 minutes followed by a second wash in tap water and then a rinse in deionized water. The Biebrich Scarlet-Acid Fuschin Stain (HT15-1) was then placed on the slides for 5 minutes followed by another rinse in deionized water. A solution of phosphotungstic/phosphomolybdic (1:1 vol/vol) acid in 2 volumes of deionized water was then placed on the slides for 5 minutes at which point the slides were transferred to an aniline blue solution (HT15-4) for 5 minutes and a 1% acetic acid solution for 2 minutes. Slides were then rinsed and dried. Images were photographed using a Leica DFC 420 CCD camera mounted on a light microscope (LEICA DM2500) operated by Image-Pro 6.2 software.

May-Grunwald Giemsa Stain

The May-Grunwald Giemsa stain (Sigma-Aldrich) was used to distinguish various cell types present in scaffold sections. The Giemsa stain was diluted 1:20 with deionized water before the slides were placed in the May-Grunwald stain for 5 minutes. They were then transferred to PBS, pH 7.2 for 1.5 minutes, followed by

treatment with dilute Giemsa solution for 15-20 minutes. The slides were briefly rinsed in deionized water, observed and photographed as described above.

Live/Dead assay

A live/ dead assay was performed according to the procedure of Thevenot [70]. Stock solutions were prepared for carboxylfluorescein diacetate, succinimidyl ester (CFDA-SE, Invitrogen; 5mM in dimethylsulfoxide) and propidium iodide (PI, Invitrogen; 1.5mM in deionized water). The explanted scaffolds were rinsed in PBS and then immersed in CFDA-SE (final concentration 2.5μM in PBS) reagent for 20 minutes at 37°C. Following this, the scaffolds were fixed in methanol for 10 minutes and stained with PI (500nM in 2x SSC [0.3M NaCl, 0.03M sodium citrate, pH 7.0]) for 5 minutes. The scaffolds were washed briefly in PBS and frozen. After imbedding in OCT and sliced as described above, the sections were examined using an Olympus IX80 laser scanning confocal microscope operated by FV1000 software v1.4a.

STATISTICAL ANALYSIS

Statistical analysis was performed using SAS 9.2 with ANOVA as well as the Student t-test for the data in Figures 2 and 3, with significance reported for $p<0.05$ or as indicated on the figure. All data (n=3) are plotted with standard error of the mean (SE).

5.0 RESULTS

5.1 Assessment of D-PHI *in vitro*

5.1.1 Establishing growth on D-PHI

To ensure the presence and examine the gross morphology of the cells on D-PHI, SEMs were taken 48 hours after culturing the cells. MCs alone (Figure 1B) and with ECs (Figure 1C) illustrate that the two cell types were viable in co-culture on D-PHI. ECs were also cultured alone and were able to form a monolayer (Figure 1A), which is suggestive of mature and functional ECs. The cells in the co-culture maintained their typical morphology while in close contact with one another (Figure 1C). Figure 2 shows phase contrast images of MC (Figure 2A), EC (Figure 2B), and co-culture (Figure 2C) on D-PHI after 7 days of culture. MC (Figure 2D), EC (Figure 2E), and co-culture (Figure 2F) are shown on TCPS after 7 days in culture as well. When examining both co-cultures it is apparent that both MCs and ECs are able to adhere to both surfaces and the ECs are able to proliferate to confluence as can be seen by the layer they have formed when cultured alone and in co-culture with MCs.

While the aim of this research was to assess D-PHI, some experiments were done using TCPS as a control in order to ensure that growth and cell attachment were taking place on D-PHI at a rate that was at least comparable to TCPS, if not better. In order to obtain a general estimation of the number of cells present on D-PHI and TCPS a DNA assay was conducted on cell lysates at 48 hours, 96 hours, and 7 days on cells cultured on both surfaces. As can be seen in Figure 3, DNA values for MC remained

relatively low and only slightly fluctuated over time. Meanwhile, the amount of DNA in the EC cultures increased on both D-PHI and TCPS over time and were comparable in number on both surfaces. A similar trend was observed in the co-culture showing the ECs were able to multiply in the presence of MCs.

The MTT assay (Figure 4) shows mitochondrial activity within cells and is therefore considered to be representative of cell number and activity. The values obtained show an increase in cell number in both the EC culture and the co-culture as would be expected while MCs remain relatively constant.

Figure 1: Scanning electron microscopy (SEM) of the EC, MC and the co-culture. Endothelial cells (A), monocytes (B), and a co-culture of ECs and MCs (C) were cultured on D-PHI for 48 hours and fixed for SEM. Fold magnification 500; scale bar 60 μm for EC, magnification 1000; scale bar 30 μm for MC and co-culture. (prepared by Joanne McBane)

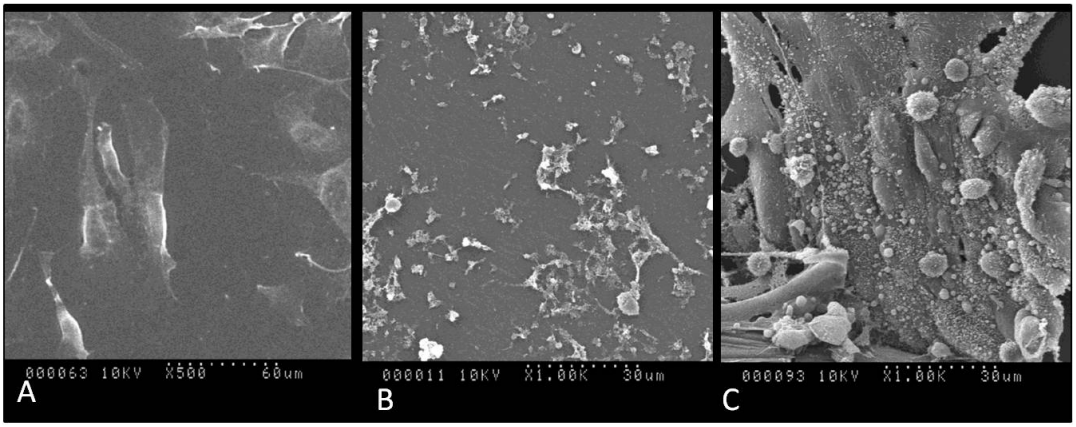
000063 10KV X500 60um
A
000011 10KV X1.00K 30um
B
000093 10KV X1.00K 30um
C

Figure 2: Phase contrast images of the EC, MC and the co-culture. MCs (A), endothelial cells (B), and co-culture (C) cultured on D-PHI for 1 week. Images of MCs (D), endothelial cells (E) and co-culture (F) cultured on TCPS for week

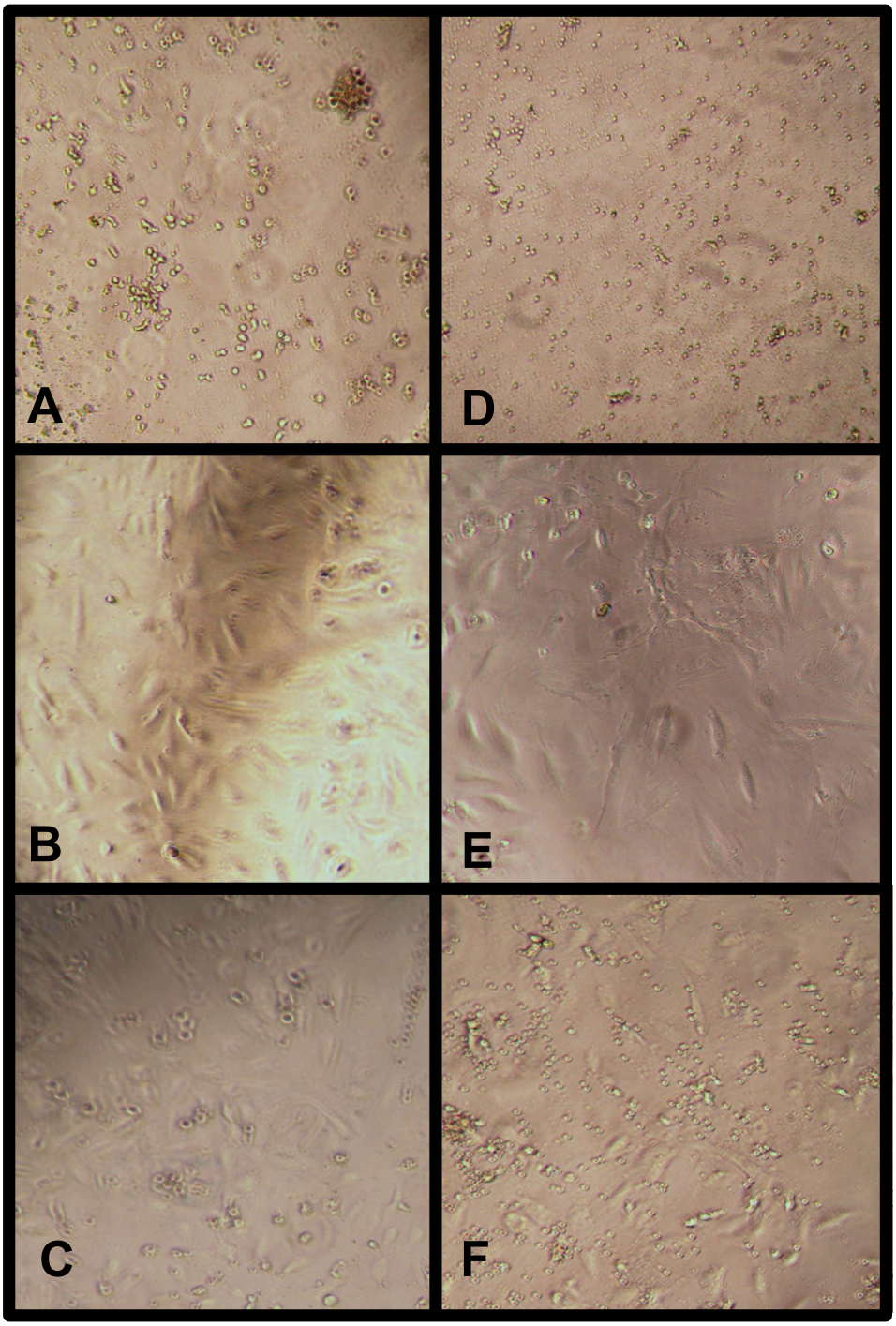
A
D
B
E
C
F

Figure 3: DNA content of lysate obtained from MC, EC and co-culture DNA assays were performed on cell lysates obtained from each cell culture at 48 hours (white), 96 hours (grey), and 7 days (black) on D-PHI and TCPS. (total ng present per well) (n=3) Data plotted +/- standard error of the mean. DNA is significantly higher at 1 week compared to 48 hours for EC culture on D-PHI and TCPS (*p=0.04, <0.0001 on each surface respectively)

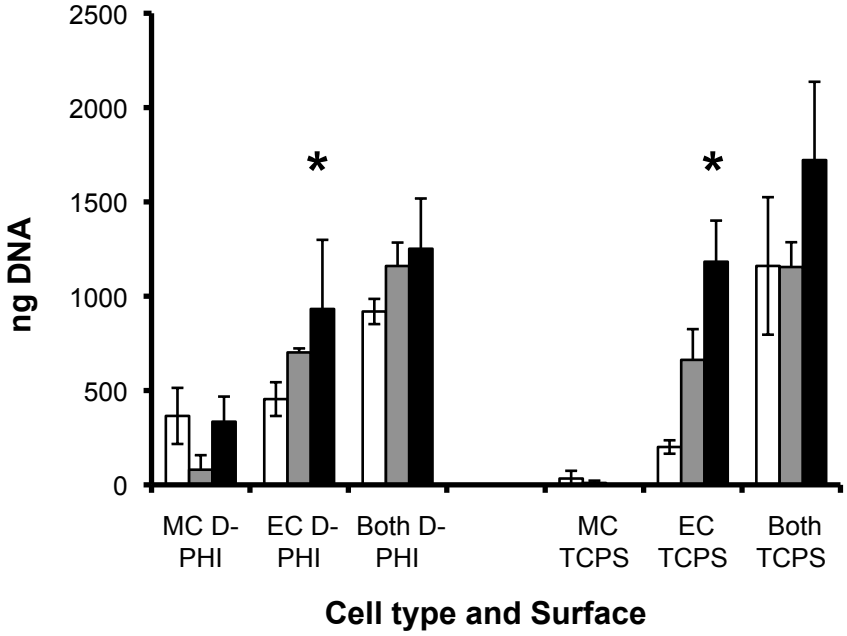
2500
2000
1500
1000
500
0
ng DNA
*
*
MC D-PHI
EC D-PHI
Both D-PHI
MC TCPS
EC TCPS
Both TCPS
Cell type and Surface

Figure 4: MTT assay for cellular proliferation. MCs, ECs, and a co-culture were cultured on D-PHI (white) and TCPS (black) and growth was measured at 48 hours and 7 days using a MTT assay. Optical density (OD) is proportional to cell proliferation and activity is shown for each set of culture conditions. (n=3) Data plotted +/- standard error of the mean

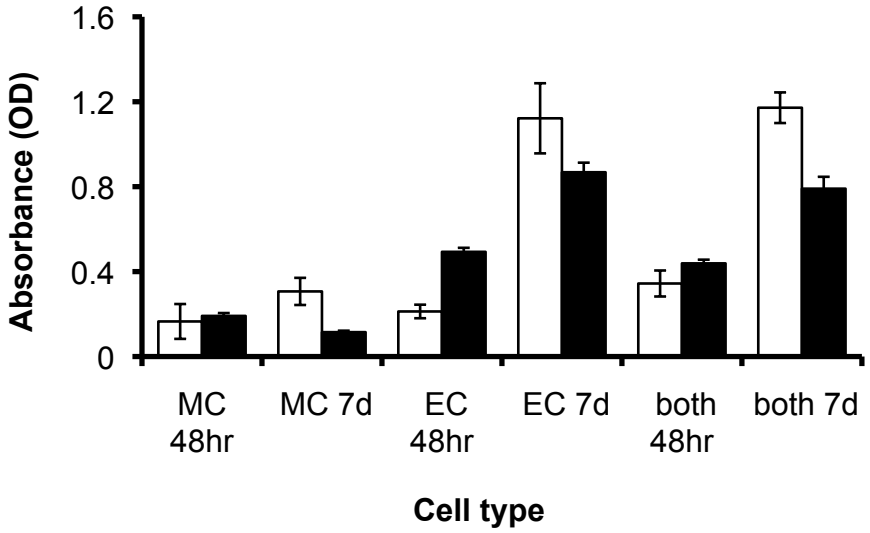
1.6
1.2
0.8
0.4
0
Absorbance (OD)
MC 48hr
MC 7d
EC 48hr
EC 7d
both 48hr
both 7d
Cell type

3.1 2 Examining cell behaviour on D-PHI

After assessing the growth qualitatively of cells with MTT, WST a water soluble tetrazolium salt, was used to assess proliferation more accurately. MTT formazan crystals formed on the D-PHI films and were difficult to solubilize in order to ensure quantitative results. Figure 5 shows the results of the WST assay where it was observed that MCs do not increase in number while the EC culture and the co-culture increased steadily and significantly over the 48 hour, 96 hour, and 7 day time points ($p< 0.05$).

Figure 6 shows the changes in esterase activity normalized to protein in cells cultured on D-PHI and TCPS for 48 hours and 7 days. While the co-culture does not display increased esterase activity compared to each cell type cultured alone, there is also significantly less esterase activity for EC and the co-culture on D-PHI as compared to TCPS ($p=0.048$, 0.05 for EC and co-culture respectively). Esterase levels in EC cultures increased significantly between 48 hours and 7 days on both D-PHI and TCPS ($p=0.0092$, 0.0006 for each surface respectively).

Immunoblotting analysis was carried out to establish that EC could maintain the functional biomarker CD31 on D-PHI and TCPS whether alone or in co-culture with MCs and this did occur (Figure 7). No CD31 was detectable in the monocyte culture alone. However, when quantitative assessment was attempted no consistent loading control could be observed. The amount of GAPDH, when loaded based on protein, varied greatly between each cell type confounding even further the quantification of any protein in the co-culture (See Appendix Figure A1).

ELISAs for TNF-α and IL-10 were conducted on releasates from MCs, ECs and the co-culture grown on D-PHI films (Figure 8) and normalized to protein. IL-10 showed the highest levels in both the MC culture and the co-culture at 48 hours and subsequently decreased by 7 days. Although not significantly different, there was a trend to a higher level of IL-10 compared to TNF-α ($p=0.09$) and both decreased over time. More important was there was no TNF-α measured in the co-culture by 7 days.

Figure 5: Assay of growth of MC, EC and the co-culture on D-PHI. The growth of MCs, endothelial cells and the co-culture on D-PHI at 48 hours (white), 96 hours (grey), and 7 days (black) was determined using a WST assay. Optical density (OD) is proportional to cell proliferation and activity is shown for each set of culture conditions. Growth increases significantly in EC culture and co-cultures between all time points *p=<0.05

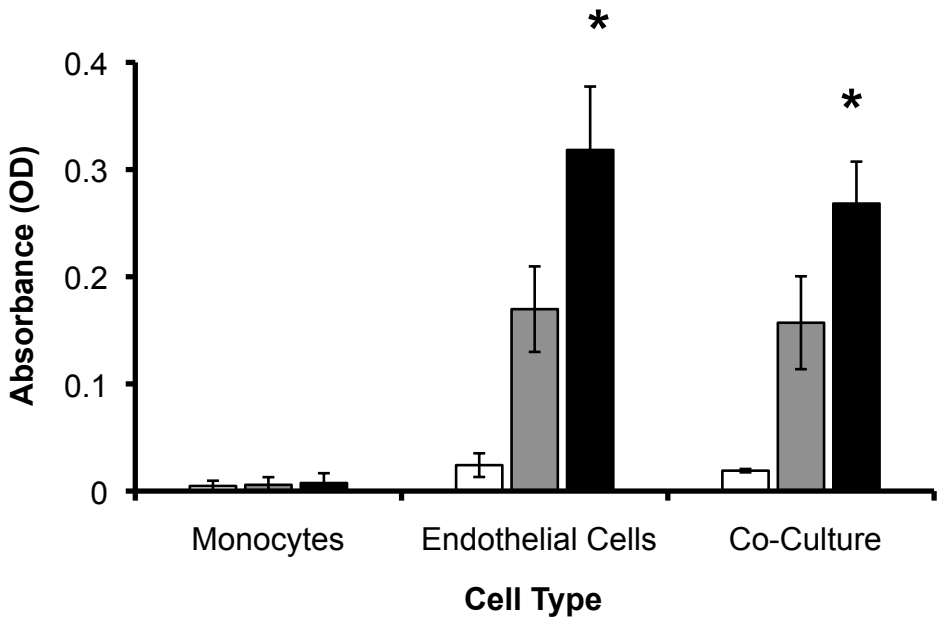
*
*
0.4
0.3
0.2
0.1
0
Absorbance (OD)
Monocytes
Endothelial Cells
Co-Culture
Cell Type

Figure 6: Esterase activity in MC, EC and the co-culture on D-PHI and TCPS. Esterase activity (nmol/min/μg protein) in cell lysates was assayed at 48 hours (black) and 7 days (white) for each surface. (n=3) Data plotted +/- standard error of the mean. Esterase activity was significantly lower for ECs and the co-culture on D-PHI compared to TCPS (*p=0.048, 0.05 for each cell type respectively). Esterase activity increased significantly in EC cultures on D-PHI and TCPS between 48 hours and 7 days (#p=0.0092, 0.0006 for each surface respectively.

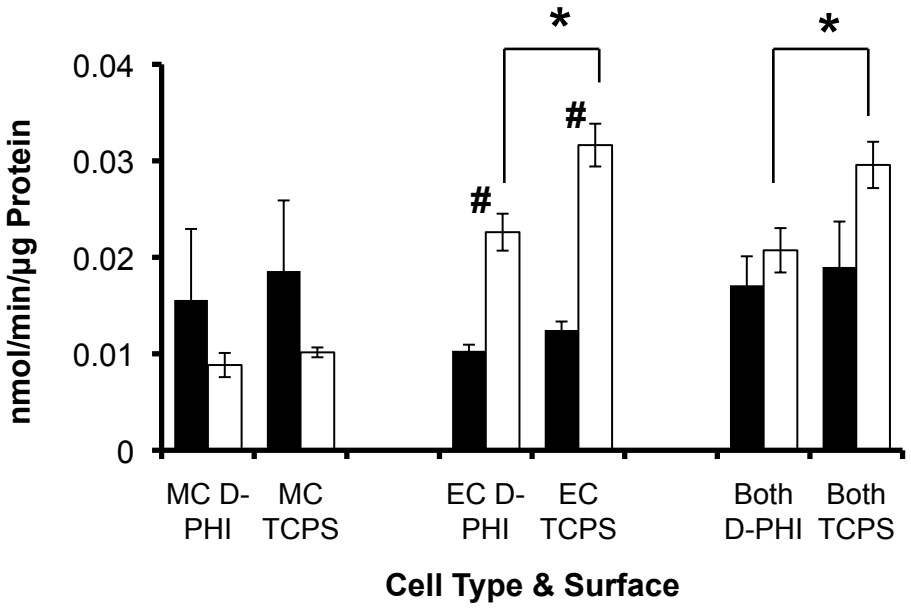
*
*
#
#
0.04
0.03
0.02
0.01
0
nmol/min/µg Protein
MC D-PHI
MC TCPS
EC D-PHI
EC TCPS
Both D-PHI
Both TCPS
Cell Type & Surface

Figure 7: Immunoblotting analysis of CD31 expression in MC, EC and the co-culture. Immunoblotting analysis was performed on cell lysates using an antibody to CD31 after 7 days in culture on D-PHI and TCPS. (prepared by Loren Matheson)

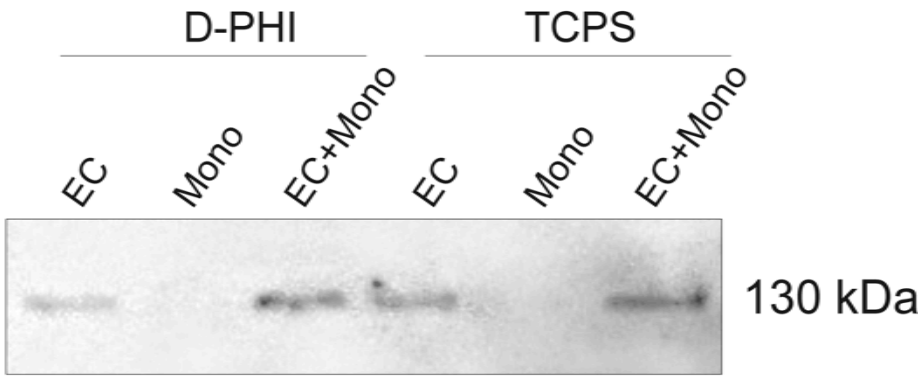
D-PHI
TCPS
EC
Mono
EC+Mono
EC
Mono
EC+Mono
130 kDa

Figure 8: Cytokine analysis of conditioned media of MC, EC and the co-culture on D-PHI by ELISA. TNF-α (white) and IL-10 (black) present in the MC, EC, and co-culture conditioned media was normalized to protein at 48 hours and 7 days and assayed by ELISA. While the levels of both cytokines decreased over time, the inflammatory cytokine TNF- α was no longer present by day 7 in the co-culture. (n=3) Data plotted +/- standard error of the mean.

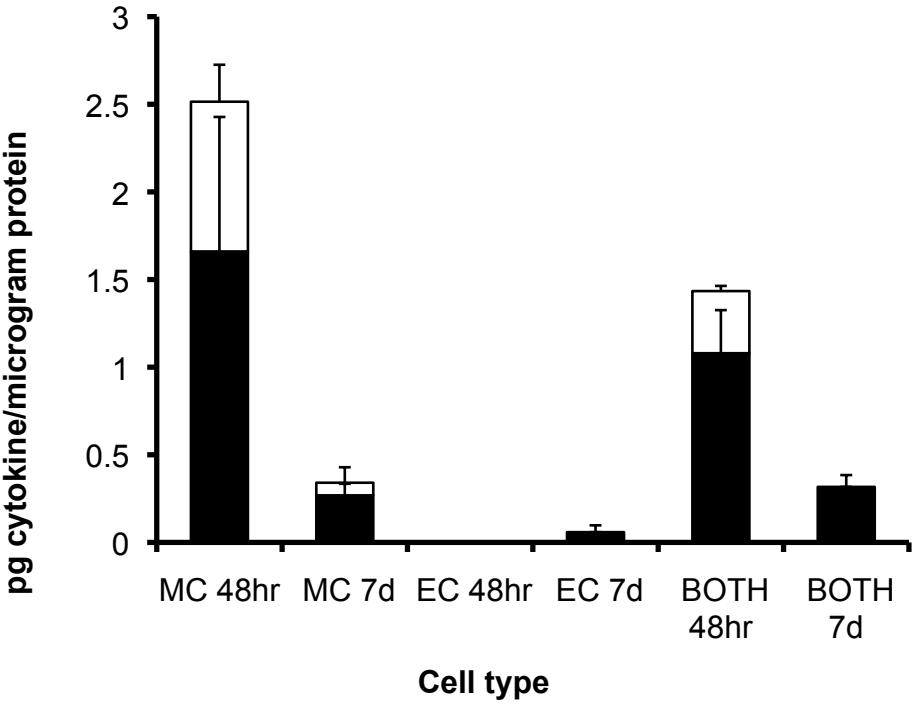
3
2.5
2
1.5
1
0.5
0
pg cytokine/microgram protein
MC 48hr
MC 7d
EC 48hr
EC 7d
BOTH 48hr
BOTH 7d
Cell type

3.2 *In vivo* assessment of D-PHI

Images and Histological analysis

In order to assess the biocompatibility of D-PHI scaffolds histological analysis and cytokine antibody arrays were conducted on the explanted scaffolds. Figure 9 depicts the site of implant of a 6 week subcutaneous scaffold implant in a mouse. As can be observed, the site of the implant has healed, hair growth returned, and no obvious inflammation was present. Upon explanting the scaffold there was good tissue integration observed and no apparent signs of an inflammatory response (heat, redness, swelling).

Figure 10 shows a SEM image of a D-PHI scaffold that was explanted following subcutaneous implantation for 2 weeks demonstrating that cells and extracellular matrix were adherent to the scaffold (A). Blood vessel growth was also observed over the surface of the scaffold (B). For comparison purposes, panel (C) shows a control scaffold, which was not implanted.

Images obtained from various histological techniques can be seen in Figure 11. Panels (A) to (D) show the results of a live dead assay with live cytoplasm staining green and nuclei red. Panels (E) and (G) show the results of the May-Grunwald stain while (F) and (H) show the scaffold alone. In panel (E) the edge of the scaffold is visible and tissue migration into the scaffold and surrounding the scaffold may be observed. Panel (G) shows tissue formation inside of the scaffold. Blue/pink staining reveals cell cytoplasm while the nuclei are varying shades of purple.

The Masson-trichrome stain was used to reveal the presence of collagen and muscle fibers in addition to cells. The deposition of collagen can be observed surrounding the scaffold in panel (I) and migrating into the scaffold in panel (K) while panels (J) and (L) show the effect of the stain on the scaffold alone in the absence of implantation. Nuclei stained black and cytoplasm stained red allowing for the detection of cells within the matrix.

Figure 9: Images of the scaffold in a subcutaneous implant in the mouse. Following a 6 week time period the scaffold structure could be seen through the epidermis. The implant site had healed and no obvious inflammation was present (see inset) (A). Following an incision the scaffold was made visible. Tissue had integrated into the scaffold and blood vessels were seen growing over the surface (see inset) (B).

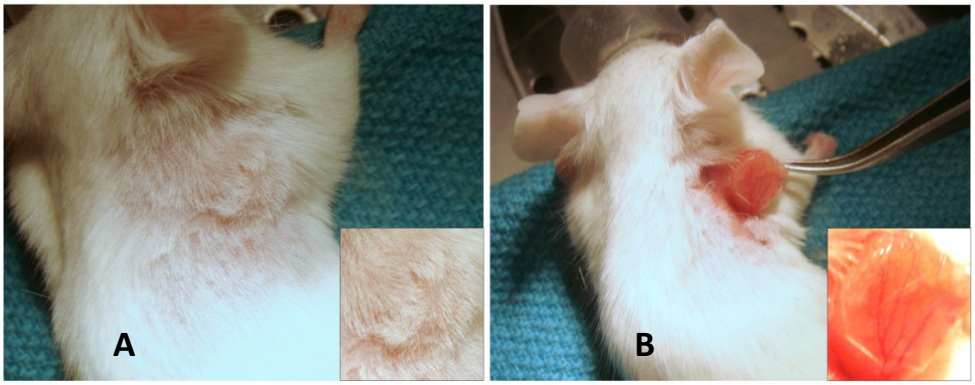
A
B

Figure 10: Scanning electron microscopy (SEM) of an explanted scaffold following a 2 week subcutaneous implant period in the mouse (A) and (B) and a control scaffold not implanted (C). Note the deposition of extracellular matrix in (A) (*) (200 x magnification) and a blood vessel growing on the surface of the explanted scaffold (B) (arrow) (500 x magnification; scale bar (A) = 150 μm; scale bar (B) and (C) = 60 μm). (prepared by Joanne McBane)

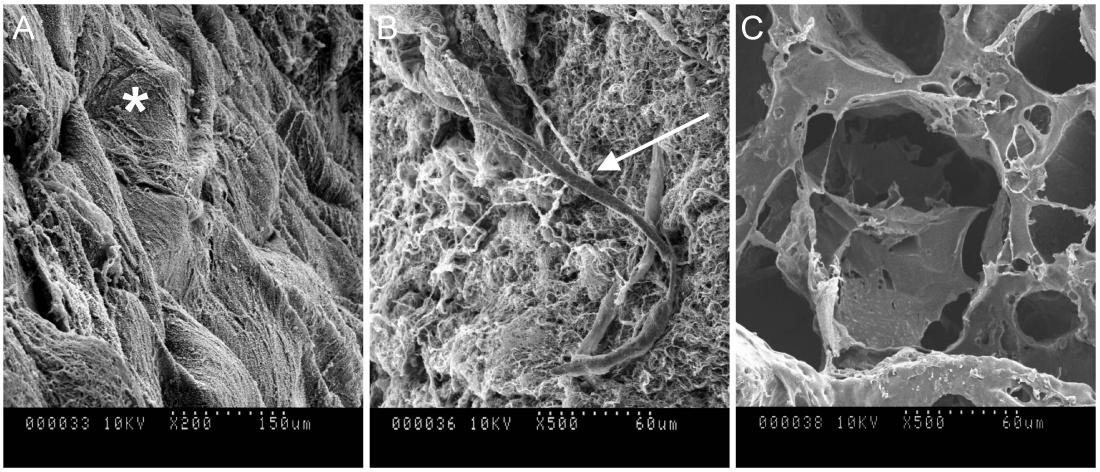
A
*
000033 10KV X200 150um
B
000036 10KV X500 60um
C
000038 10KV X500 60um

Figure 11: Histological assessment of explanted scaffolds for cell viability and tissue in growth after 1 week. A live-dead fixed assay showed the cytoplasm of live cells stained green (A), nuclei red (B) and overlay (C). (E) and (G) showed the explanted scaffold stained with May-Grunwald Giemsa. Panels (I-L) show the Masson-trichrome stain. (scale bar = 100 μm) (prepared by Loren Matheson)

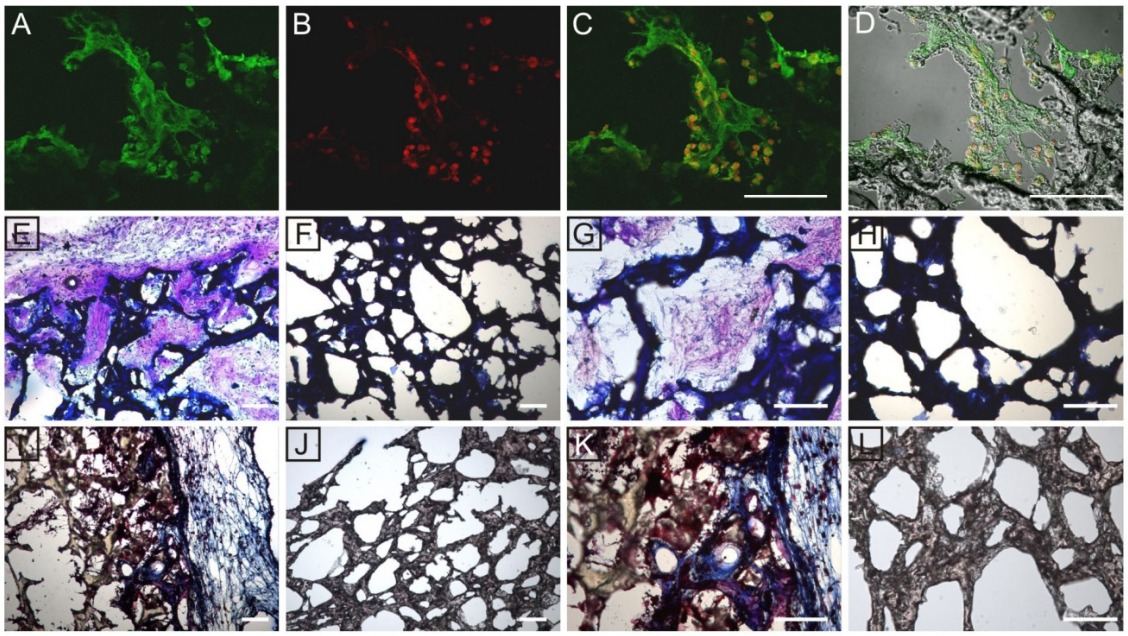
A
B
C
D
E
F
G
H
I
J
K
L

Inflammatory Cytokine Profile

The first set of cytokine analysis data were completed for *in vivo* implants explanted at a 1 week time point and compared to plasma from a healthy mouse as a control. These values were all normalized to TNF-α in order to produce Figure 12 (MCP-5 is significantly greater, (MCP-5,* p = 0.01; MCP-1, # p = 0.09);) and it was decided that more time points should be completed in order to better understand the fluctuation of cytokines over time.

The various cytokines examined at 24 hours, 1 week, 2 weeks, 4 weeks, and 6 weeks allowed us to gain perspective on the inflammatory response induced in the mouse by the scaffolds. All values were obtained as intensities normalized to internal positive controls which were present on each scaffold. The ratio of each cytokine was then normalized to the same cytokine average value obtained from 24 hours. As such, all results are a ratio, which allowed visualization of the relative levels of each cytokine at defined time points over a 6 week time period.

When examining Figure 13, we see that MCP-5 peaked at 1 week but then decreased in amount, while MCP-1 was much greater in quantity by 6 weeks. MCP-5 was significantly higher at 1 week as compared to 24 hours, 4 weeks and 6 weeks (*p=0.0013, 0.0075, 0.0266). MCP-1 was significantly higher at 6 weeks as compared to all of the other time points (#p= <0.0001, 0.0003, 0.0021, 0.0006).

Figure 14 shows levels of IL-12p40p70, which increased over time. IL-12p40p70 was significantly higher than the other time points by 4 (#p=0.0044, 0.0098, 0.0286) and 6 weeks (*p=0.0002, 0.0003, 0.0007, 0.0491).

Figure 15 shows levels of GM-CSF which peaked at 1 week (significantly higher than at 24 hours (*p=0.0410)) but then decreased again although these values were not significant.

Figure 16 shows IL-6 where later time points were significantly lower than at 24 hours (*p=<0.0001).

Figure 17 shows levels of regulated on activation normal T cell expressed and secreted protein (RANTES) which displayed a trend of increasing over time with significantly more at 4 weeks and 6 weeks than at the other 3 time points; (4 (#p=0.0013, 0.016, 0.0374) and 6 weeks (*p=0.0002, 0.0023, 0.0053) respectively).

Figure 18 shows TNF-α and its antagonist sTNF-R1. While TNF-α levels showed a large amount of variability, they did not exceed the amount present at 24 hours. In contrast sTNF-RI levels showed a trend of increasing over time, where the levels were significantly higher at 4 and 6 weeks; 4 (#p= 0.0337) and 6 weeks (*p=0.0063 respectively).

In Figure 19 IL-10 and IL-13, two anti-inflammatory cytokines are displayed. While these cytokines fluctuated greatly over time, by 6 weeks they showed significantly greater amounts (~ 8 x for IL-10, ~ 6 x for IL-13) (*p= 0.0021 for IL-10 and #p=0.0357 for IL-13).

Figure 20 shows IL-10 and TNF-α data presented as stacked bars. These data are taken from Figure 18 and 19 but presented differently to show that by 6 weeks IL-10 is significantly higher ($p= 0.0021$) and TNF-α shows a trend towards decreasing compared to 24 hours.

Figure 12: Cytokine antibody array of proteins on scaffolds explanted after 7 days (black bars) and in normal mouse plasma (grey bars). Cytokine levels were expressed as a ratio to TNF-α; (MCP-5,* $p = 0.01$; MCP-1, # $p = 0.09$); (n=3) Data plotted +/- standard error of the mean.

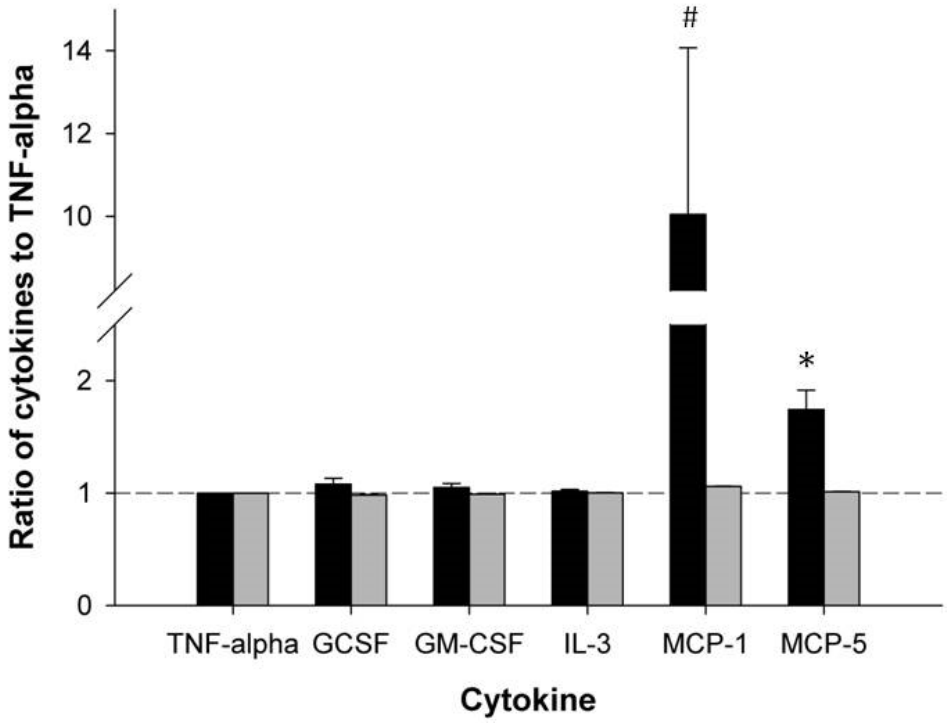
Ratio of cytokines to TNF-alpha
14
12
10
2
1
0
#
*
TNF-alpha
GCSF
GM-CSF
IL-3
MCP-1
MCP-5
Cytokine

Figure 13: Cytokine antibody array of lysate from explanted scaffolds. Levels of MCP-5 (grey square) and MCP-1 (black circle) normalized to internal controls and then calculated as a ratio to their respective values at 24 hours (equals 1). MCP-5 was significantly higher at 1 week as compared to 24 hours, 4 weeks and 6 weeks (*p=0.0013, 0.0075, 0.0266). MCP-1 was significantly higher at 6 weeks as compared to all of the other time points (#p= <0.0001, 0.0003, 0.0021, 0.0006). (n=3)

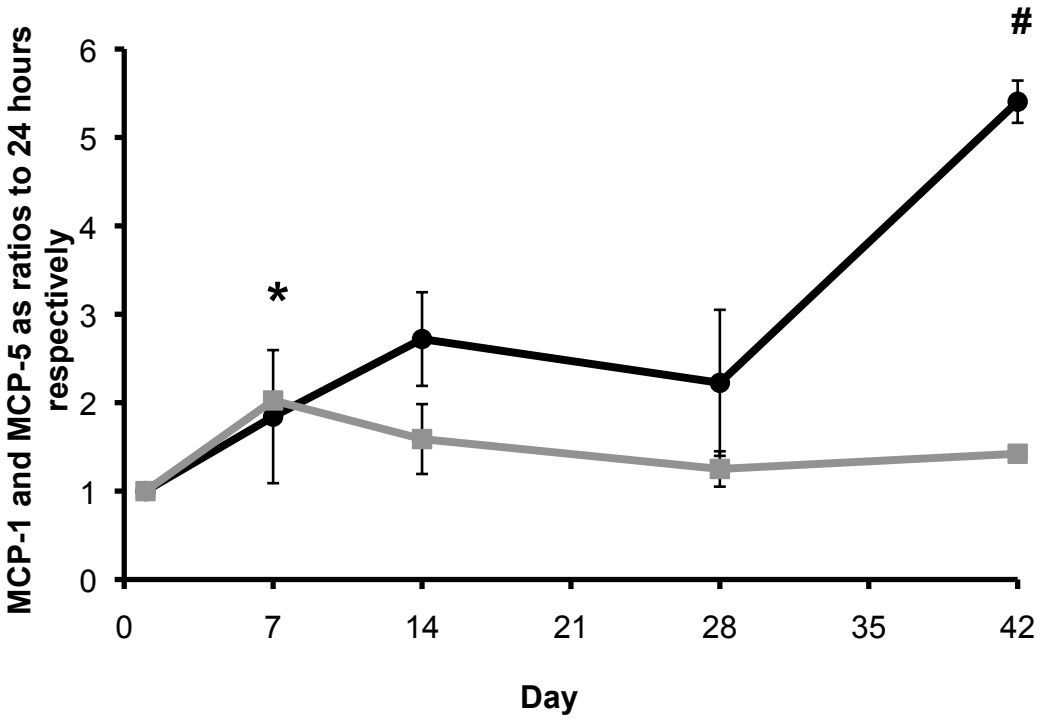
MCP-1 and MCP-5 as ratios to 24 hours respectively
6
5
4
3
2
1
0
*
#
0
7
14
21
28
35
42
Day

Figure 14: Cytokine antibody array of lysate from explanted scaffolds. Levels of IL-12p40p70 (black circle) were normalized to internal controls and then calculated as a ratio to 24 hours (equals 1). IL-12p40p70 was significantly higher than the other time points by 4 (#p=0.0044, 0.0098, 0.0286) and 6 weeks (*p=0.0002, 0.0003, 0.0007, 0.0491) (n=3)

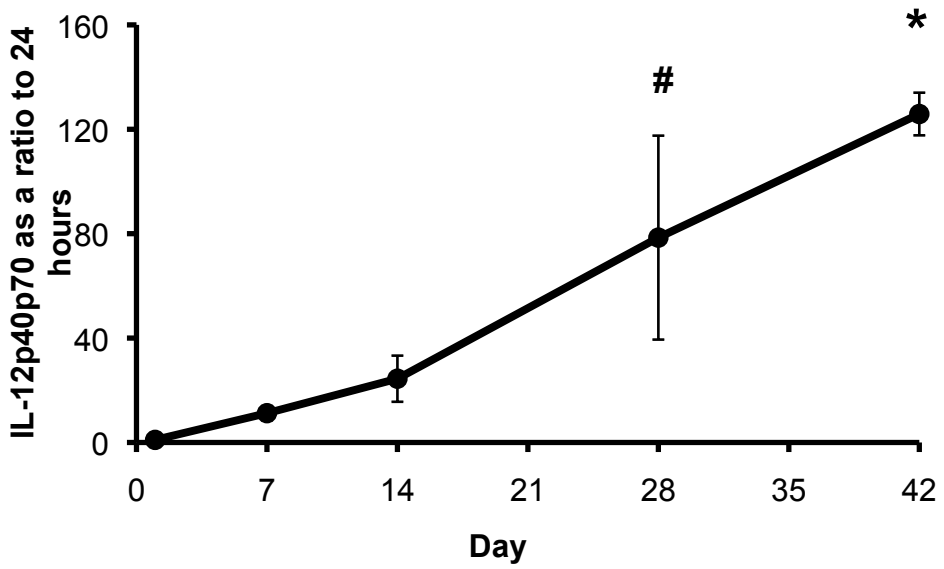
IL-12p40p70 as a ratio to 24 hours
160
120
80
40
0
0
7
14
21
28
35
42
Day
#
*

Figure 15: Cytokine antibody array of lysate from explanted scaffolds. Levels of GM-CSF (black circle) were normalized to internal controls and then calculated as a ratio to 24 hours (equals 1). GM-CSF was significantly higher than 24 hours after 1 week (*p=0.0410) (n=3)

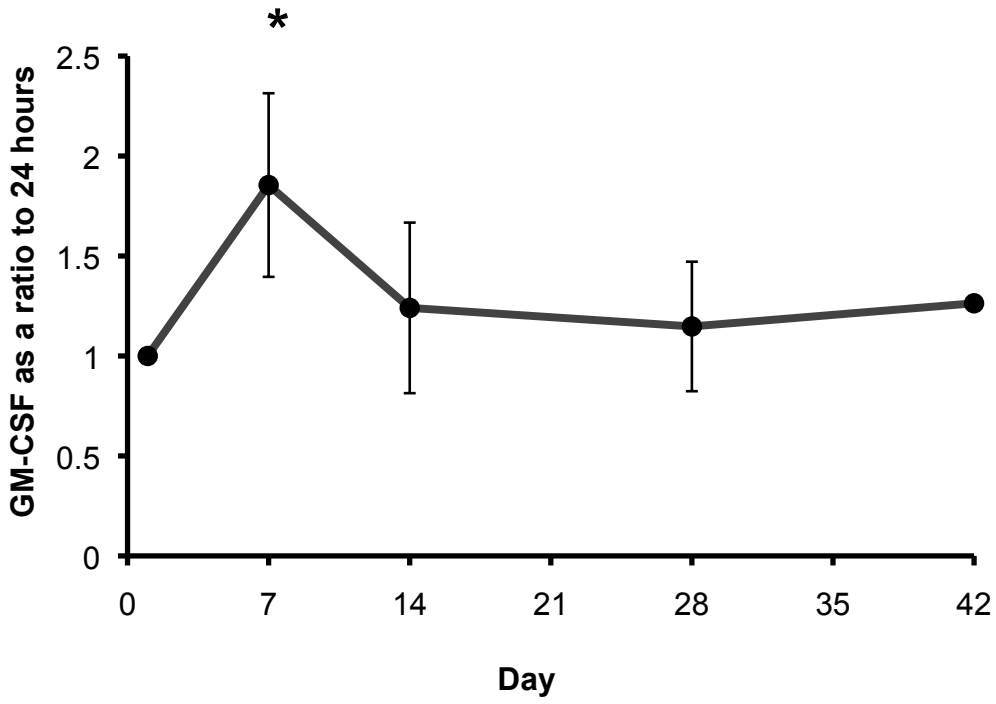
*
GM-CSF as a ratio to 24 hours
2.5
2
1.5
1
0.5
0
0
7
14
21
28
35
42
Day

Figure 16: Cytokine antibody array of lysate from explanted scaffolds. Levels of IL-6 (black circle) were normalized to internal controls and then calculated as a ratio to 24 hours (equals 1). IL-6 is significantly higher at 24 hours than any other time point (*p=<0.0001) (n=3)

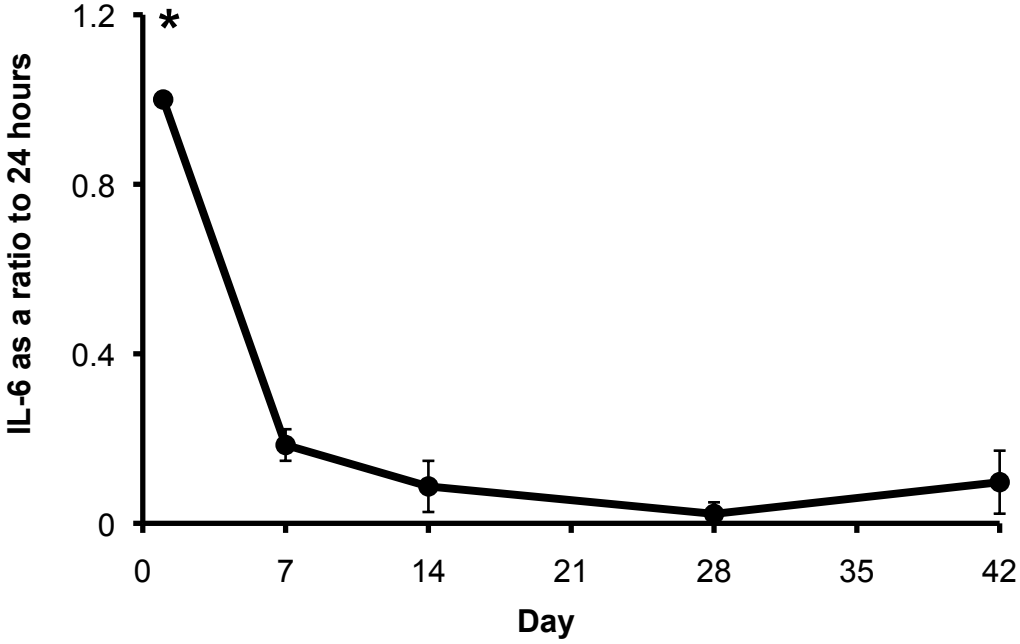
1.2
0.8
0.4
0
*
IL-6 as a ratio to 24 hours
0
7
14
21
28
35
42
Day

Figure 17: Cytokine antibody array of lysate from explanted scaffolds. Levels of RANTES (black circle) normalized to internal controls and then calculated as a ratio to 24 hours (equals 1). RANTES was significantly higher 4 (#p=0.0013, 0.016, 0.0374) and 6 weeks (*p=0.0002, 0.0023, 0.0053) than any other time point. (n=3)

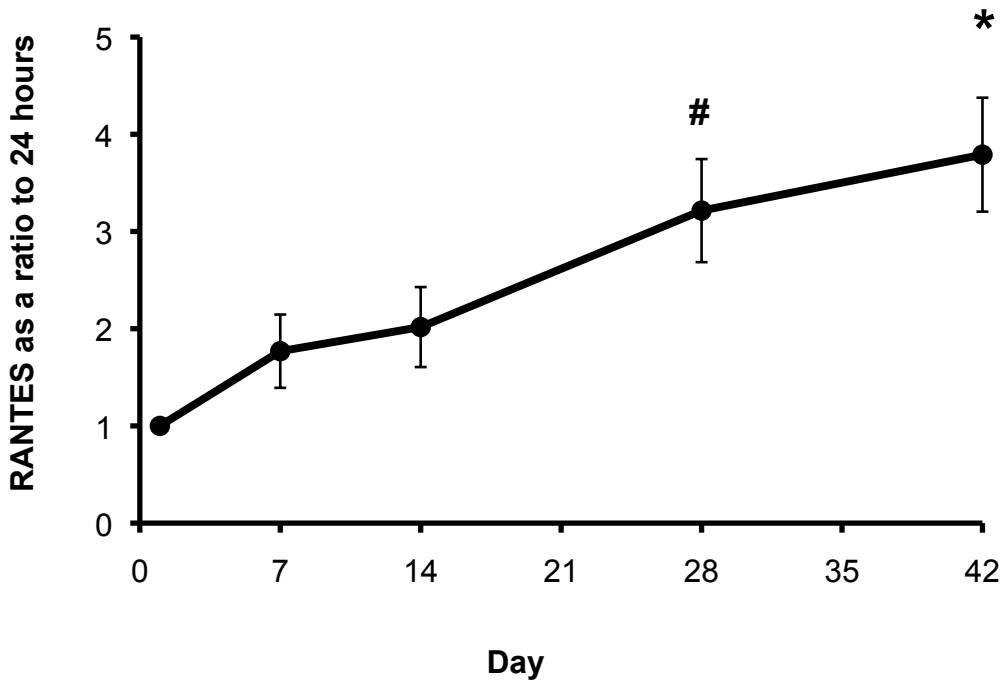
RANTES as a ratio to 24 hours
5
4
3
2
1
0
0
7
14
21
28
35
42
Day
#
*

Figure 18: Cytokine antibody array of lysate from explanted scaffolds. Levels of TNF-α (black circle) and sTNF-RI (grey square) normalized to internal controls and then calculated as a ratio to their respective values at 24 hours (equals 1). sTNF-RI was significantly higher than 24 hours by 4 (#p= 0.0337) and 6 weeks (*p=0.0063). (n=3)

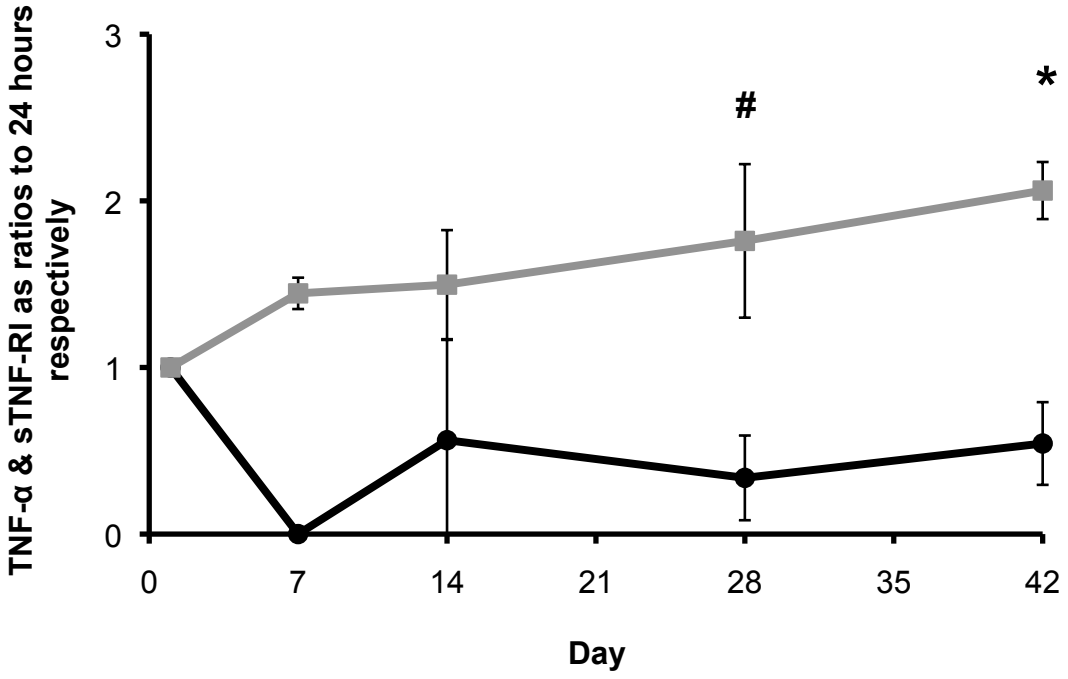
TNF-α & sTNF-RI as ratios to 24 hours respectively
3
2
1
0
0
7
14
21
28
35
42
Day
#
*

Figure 19: Cytokine antibody array of lysate from explanted scaffolds. Levels of IL-10 (black circle) and IL-13 (grey square) normalized to internal controls and then calculated as a ratio to their respective values at 24 hours (equals 1). IL-10 (*p= 0.0021) and IL-13 (#p0.0357) are both significantly higher by 6 weeks as compared to 24 hours. (n=3)

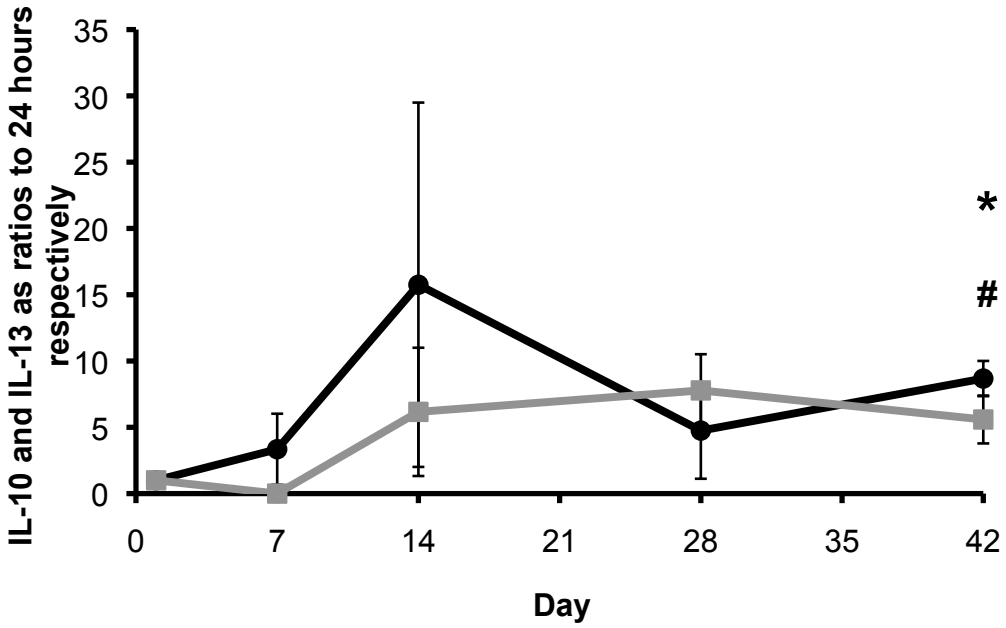
IL-10 and IL-13 as ratios to 24 hours respectively
35
30
25
20
15
10
5
0
0
7
14
21
28
35
42
Day
*
#

Figure 20: Cytokine antibody array of lysate from explanted scaffolds. Stacked bar graph showing relative levels of TNF-α (white) and IL-10 (black) normalized to internal controls then calculated as a ratio to their respective values at 24 hours (equals 1) and 6 weeks. While IL-10 levels significantly increase ($p= 0.0021$)., TNF-α levels do not. (n=3)

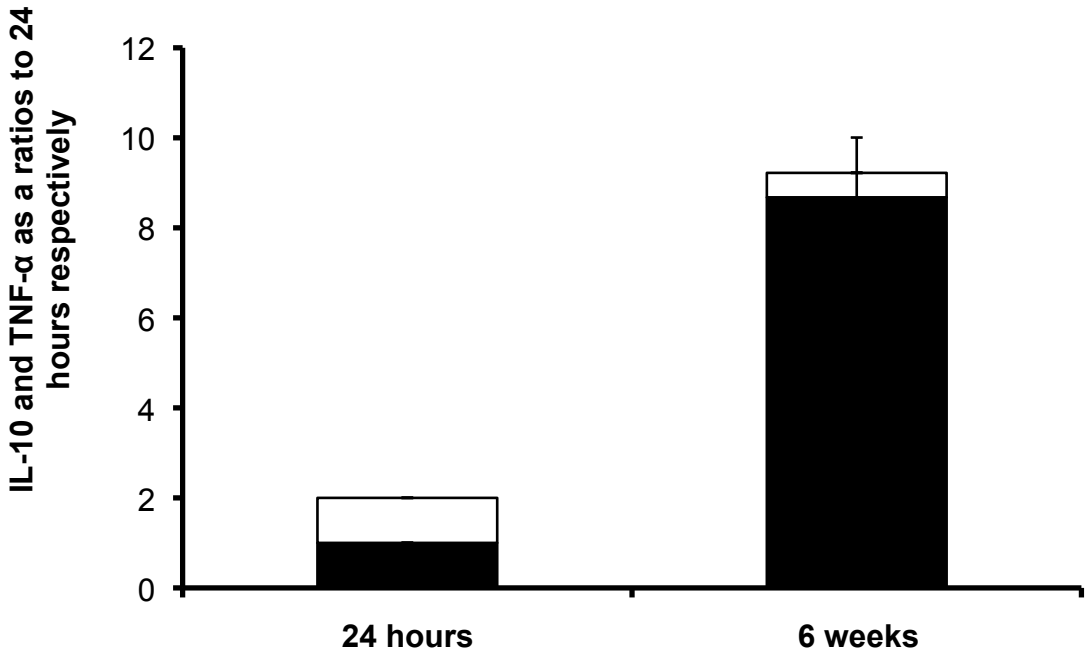
IL-10 and TNF-α as a ratios to 24 hours respectively
12
10
8
6
4
2
0
24 hours
6 weeks

6.0 DISCUSSION

Using the carefully constructed D-PHI in the form of both non-porous, solid discs and porous scaffold discs, experiments were carried out in order to assess the suitability of the material for future construction of a small diameter peripheral artery vascular graft by examining cell compatibility and growth both *in vitro* and *in vivo*. Specifically, the objectives were to characterize D-PHI films *in vitro* with an EC/monocyte co-culture and *in vivo* with a porous scaffold implanted in a mouse subcutaneous model.

6.1 *In vitro* Analysis of D-PHI

The purpose of this part of the study was to assess growth, esterase activity and cytokine production in an EC/MC co- culture on D-PHI films *in vitro.* An *in vitro* system was developed with a special focus on the MC and EC response to the material as well as the development of a co-culture of the two cell types to better simulate the *in vivo* conditions. These studies assessed growth, esterase activity and cytokine production in an EC/MC co- culture on D-PHI films *in vitro*.

Establishing a co-culture of human ECs and human MCs had to be completed prior to the initiation of the *in vitro* component of this project. In order to accomplish this, preliminary experiments were conducted both on D-PHI and tissue culture polystyrene (TCPS). As cells are generally cultured on TCPS this was considered a suitable control with which to compare their behaviour on D-PHI. After examining different variables and conditions (media composition and cell seeding densities) co-culture conditions were established. Human endothelial cells were seeded 24 hours prior to the addition of peripheral blood mononuclear cells (PBMCs). Since the ECs are able

to divide rapidly while adherent MCs do not proliferate, it was decided that the cells would be seeded in a 3:1 ratio of MCs to endothelial cells, with a varying number of total cells depending on the requirements of the experiment. ECs were seeded first in order to give them time to adhere to the surface and begin their formation of a monolayer before the addition of the PBMCs which would compete for space. This was also a better method for simulating the innate immune response where MCs would be recruited to the foreign body surface over time. After testing different combinations of media it was determined that a 50:50 mixture containing the medium of preference for MCs, RPMI, and the medium of preference for the EC, EBM-2 (Clonetics), was adequate to grow both cell types in co-culture. It was this combination of media which was used for culture conditions for all *in vitro* experiments.

It was important to ensure that the ECs were able to proliferate on D-PHI and form a confluent monolayer and it was necessary to ensure that the two cell types could grow together while maintaining their phenotype. This analysis was accomplished by culturing MC and EC separately and together and assessing cell attachment and EC growth by imaging the cells, assaying the DNA in the cell lysates and performing an MTT assay on cells cultured on D-PHI and TCPS. SEMs show cell morphology on D-PHI at 48 hours (Figure 1) while phase contrast images taken at 1 week (Figure 2) show MC and EC on both D-PHI and TCPS alone and in co-culture were adherent and/proliferating respectively.

Due to the fact the MCs do not divide while ECs do, DNA was not considered the most accurate method of estimating EC number whereas previously it was shown that DNA correlates directly with adherent MDM [67]. However, preliminary experiments

involved examining DNA content of cell lysates at 48 hours, 96 hours and 7 days on both D-PHI and TCPS to determine that cells were behaving similarly on each surface with regards to adhesion and proliferation. As predicted, DNA remained constant in MC cultures while increasing in a temporal fashion in the EC and co-cultures (Figure 3). The data obtained from the MTT assay (Figure 4), confirmed these results where for MC the value remained constant while for the ECs and co-cultures increased over time. By 7 days the growth on MTT appeared greater on D-PHI as compared to TCPS. Due to the nature of this assay and the surface of D-PHI, the formazan crystals produced (which were proportional to growth) adhered to the surface and did not dissolve sufficiently for accurate reading in the plate reader. However, these results, combined with those of the DNA assay in Figure 3 were sufficient for us to conclude that growth on D-PHI was adequate, if not better than that on TCPS. Growth, as metabolic activity, was measured again more accurately using the WST assay which produced a soluble formazan salt and could be read in a microplate reader where absorbance was directly related to the number of cells present. For this experiment D-PHI was the only surface examined and showed an increase in cell number over time (Figure 5). D-PHI allowed for good cell adhesion and viability with a significant increase in the proliferation of ECs during the 1 week culture period (~13 fold ($p<0.05$)). Monocyte mitochondrial activity remained constant over the 48 hour, 96 hour, and 7 day time points as previously shown [71].

Another important parameter when establishing co-cultures on biomaterials that are intended for use in degradable tissue engineering constructs includes the cells' esterase activity. Esterase activity in MDM has been shown to be linked to the degradation of polyurethanes and has been used as a marker of degradative potential [72,

73] in addition to being a marker of cell activation and several pathological conditions [74]. Figure 6 shows the changes in esterase activity normalized to protein in cells cultured on D-PHI and TCPS for 48 hours and 7 days. Controlled degradation of the scaffold for a potential vascular graft is necessary; however, if degradation occurs prior to repopulation of the graft, successful tissue regeneration would not occur. Ongoing work has shown that the scaffold degrades relatively slowly *in vitro* (12% after 120d) and at a controlled rate *in vivo* (21% by 100d) [75]. As was previously found with MCs alone [3], esterase activity did not increase significantly in the co-culture between 48 hours and 7days. There was however, a significant increase in the esterase activity associated with the EC cultured alone between these two time points (~30%, $p<0.05$). While esterase activity may not be traditionally associated with ECs, nonspecific esterolytic activities have been noted in Weibel-Palade bodies, on the external surface of the plasma membrane and on cytoplasmic lipid bodies in aortic EC [76]. And although it is esterase activity that has been shown to be the most degradative to polyurethanes [77], the esterolytic activity of serine proteases (which exist in all cell types) has been shown to have some degradative potential as well [78]. At neither time point did the co-culture lysate have significantly increased esterase activity when compared to EC alone. This shows that the cells were not experiencing undue activation as assessed by this biomarker in co-culture and it also suggests that the material, once implanted, would not undergo rapid hydrolytic degradation, resulting in premature failure. It is important that the scaffold of a vascular graft remain intact until repopulation of the graft with appropriate cells occurs [21], [79]. For this reason it is also important to note that there was

significantly less esterase activity on D-PHI as compared to TCPS at 7 days for the EC culture and the co-culture demonstrating that D-PHI is less activating than TCPS.

A noteworthy finding of the *in vitro* studies was established through immunoblotting analysis, which showed that the ECs maintained their CD31 marker when cultured alone and in co-culture with MCs on D-PHI (Figure 7 whereas no CD31 was detectable in the monocyte culture alone. Since CD31 is indicative of adherent, functional EC which have formed a confluent layer [80], [81] the data suggest that culturing EC with MCs on D-PHI has no negative effect on EC maturation. It was very difficult to find a loading control in order to quantify the amount of CD31 in the ECs and compare it to the co-culture. For example, GAPDH varied greatly as a percent of total cell protein between the MC which did not divide and EC which did (see appendix Figure A1 A, B). An important finding was that the CD31 expressed in the co-culture was not due to EC interaction with MC causing MC to de-differentiate When MCs were cultured in conditioned media removed from ECs cultured for 1 week in EBM-2 and mixed 50:50 with RPMI these cells did not show any CD31 expression when cultured for 1 week (see appendix figure A1B). This shows that MCs were able to maintain their phenotype when exposed to signals released into the local cellular environment by ECs.

ELISAs for TNF-α and IL-10 were conducted on conditioned media from MCs, ECs and the co-culture grown on D-PHI films (Figure 8). While TNF-α is associated with the inflammatory response, IL-10 is a recognized anti-inflammatory cytokine marker [82]. IL-10 showed the highest levels in both the monocyte culture and the co-culture at 48 hours and subsequently decreased by 7 days. Although not significantly different, there was a trend to a higher level of IL-10 compared to TNF-α ($p=0.09$) and both

decreased over time. An important observation was that no TNF-α could be measured in the co-culture by 7 days. These results support the anti-inflammatory phenotype of the MCs on D-PHI. A previous study has shown that IL-10 has anti-inflammatory effects on monocyte/endothelium interactions and may actually be produced as a result of these interactions [83, 84].

6.2 *In vivo* analysis of D-PHI

The purpose of the *in vivo* analysis of D-PHI was to assess the inflammatory response activated by D-PHI in scaffold form when implanted *in vivo* in a mouse subcutaneous model using histological techniques to examine tissue in-growth and cytokine antibody arrays to assess biocompatibility. An important initial step when examining a material intended for graft use is to determine the inflammatory response initiated when the material is implanted and ensure that it is not severe [30]. Cytokine profiles from the explanted scaffolds provided greater detail on the manner in which the implant had integrated with the host tissue, as well as the study of the specific inflammatory pathway activation. Histological analysis provided data regarding cell recruitment to the implant, extracellular matrix formation, tissue infiltration, and cell viability.

In the initial *in vivo* studies, the scaffolds were implanted for three time points (1, 2 or 6 weeks) with no evidence of infection, inflammation or discomfort observed at any time. The scaffold prior to explanation following a 6 week *in vivo* period is shown in Figure 9A and was completely healed (Figure 9A inset). The explanted scaffold, still attached to the surrounding tissue (Figure 9B), was well integrated and showed that blood vessels were clearly visible (Figure 9B, inset).

The SEM image of a D-PHI scaffold that was explanted following subcutaneous implantation for 2 weeks (Figure 10 demonstrated that cells and extracellular matrix were adherent to the scaffold (panel A), as predicted. Blood vessel growth was also observed over the surface of the scaffold (panel B).

Figure 11 shows the results for the histological analysis of the tissue in-growth (extracellular matrix, cells) as well as the cell viability within the scaffolds. Panels (A-D) show images obtained from the live/dead assay and confirmed that the cells present within the scaffold were in fact viable. Cells have migrated into the pores of the structure while maintaining their viability. No dead cells were visible in the sections, supporting D-PHI's ability to support cell viability. This also ensured that the cytokine arrays were being performed on what was produced by live cells.

Panels (E) and (G) show the results of the May-Grunwald stain demonstrating that tissue migration into the scaffold and surrounding the scaffold was taking place. The May-Grunwald Giemsa stain has previously been shown by others to effectively demonstrate differential staining of tissues from that of polyurethanes [85]. The findings confirm that within one week, tissue integration within the scaffold was extensive and that tissue integration with the scaffold was effective.

The Masson trichrome stain was used to reveal the presence of collagen and muscle fibers in addition to cells and has been applied extensively to show tissue in-growth in synthetic vascular grafts [86, 87]. The deposition of collagen can be observed surrounding the scaffold in panel (I) and migrating into the scaffold in panel (K).

Figure 12 was included as it is was obtained from preliminary *in vivo* experiments which were conducted using plasma as a control and only a 1 week time point explant.

When pro-inflammatory cytokine values such as GCSF, GM-CSF, or IL-3 in lysates were calculated as a ratio to TNF-α for comparison to normal plasma, there were no significant changes. There was, however, an observation of increased chemoattractant factors in the tissue lysates when compared to normal plasma, with MCP-1 being up-regulated by ~850% ($p=0.09$) and MCP-5 by ~70% ($p=0.01$). Taken together with the low production of the selected pro-inflammatory cytokines, the observed up-regulation in MC chemoattractants may indicate that the MCs that are being drawn to the scaffold had a low inflammatory state which could favour wound-healing. However, this figure did not provide sufficient information which was why the experiment was repeated using more time points and normalizing each cytokine to its own value at 24 hours in order to observe fluctuations in cytokine levels over time.

The profile of the cytokines produced by cells in the local tissue and/or those which migrated into the scaffold following implantation generally supported the concept of a low inflammatory mechanism in response to D-PHI. Figure 13 shows the data for MCP-1 and MCP-5 with MCP-5 being significantly higher at 1 week and MCP-1 significantly higher at 6 weeks. As mentioned in Section 1.0, it has been shown that MCP-1 significantly increases the level of perfusion in an ischemic porcine hindlimb [54]. When considering this along with the low production of selected pro-inflammatory cytokines observed, the up-regulation in these monocyte chemoattractants may indicate that the MCs that are being drawn to the scaffold have a low inflammatory state which could favor wound healing.

When examining Figure 14 we see a trend of increasing IL-12p40p70 with significantly more present at 4 and 6 weeks. While limited information is available on

this cytokine, it has been shown to increase with infection [88]. This is to be expected as the mouse's immune system is recognizing the material as foreign. Figure 15 shows a peak of GM-CSF at 1 week which is significantly greater than at 24 hours. GM-CSF has the ability to stimulate the differentiation and function of granulocytes, MCs, and macrophages [89] which is to be expected following the implantation of a foreign material. However, this response diminished after 1 week showing it was curbed following an initial activation.

What is of considerable importance can be seen when examining Figure 16 which shows significantly higher levels of IL-6 at 24 hours which subsequently decreased dramatically. IL-6 is produced at the site of inflammation and has an important role in the acute phase of inflammation and in stimulating chronic inflammation [90]. The fact that it decreased over time was beneficial in avoiding continuous inflammation at the site of the implant.

Data for RANTES can be seen in Figure 17 and shows a trend towards increasing over time with significantly more present at 4 and 6 weeks. This is considered a proinflammatory chemokine which promotes the accumulation and activation of cells during inflammatory conditions [91]. While not ideal, it is expected that this response will be triggered when a foreign material is implanted and must be considered relative to the levels of the anti-inflammatory cytokines that may modulate its pro-inflammatory response.

Results for TNF- α in Figure 18 were encouraging and helped to prove the hypothesis that D-PHI supports an anti-inflammatory phenotype. Although not significant, all TNF- α values were less than those at 24 hours showing that a large

inflammatory response was not being initiated. TNF- α is considered a major mediator of inflammation and mediates diseases ranging from cancer, to arthritis to atherosclerosis through its ability to activate the transcription factor NF-kappaB [92]. Meanwhile, in Figure 18 we see an increasing trend in the levels of sTNF-RI, which is significantly greater at the 4 and 6 week time points than at any other time point. Studies have shown that sTNF-RI is likely part of an anti-inflammatory pathway whereby it signals a protective mechanism to tissues from disease [93]. Taking the relative levels of these two cytokines into account, it appears that an anti-inflammatory, wound healing process could likely be underway.

Figure 19 shows levels of IL-10 and IL-13, two cytokines with known anti-inflammatory properties. IL-10 has been shown to regulate activated macrophages and antigen-presenting cells through decreasing cytokine and chemokine production from macrophages and dendritic cells, ultimately limiting chronic and acute inflammation [94]. IL-13 has been shown to have similar abilities to IL-10 in down regulating an inflammatory response, although less potent than IL-10 which is still considered the most active anti-inflammatory cytokine [95].

Figure 20 is simply a different way of presenting the TNF- α and IL-10 data but it agrees well with the findings in the *in vitro* portion of this thesis. As time progresses the amount of TNF- α is negligible while the anti-inflammatory IL-10 is significantly increased.

7.0 CONCLUSION

This study has demonstrated that the D-PHI material, whether in film (*in vitro*) or scaffold (*in vivo*) form, invoked a response which included low levels of inflammation while allowing for cell viability and growth. *In vitro* cell culture results supported the hypothesis that the culture of MCs in co-culture with ECs on D-PHI films would promote a functional EC layer (CD31 expression) and significant EC growth. While the anti-inflammatory cytokine IL-10 was released in the *in vitro* co-culture at 7 days, there was no detectable pro-inflammatory cytokine TNF-α at that time thereby maintaining the low inflammatory state. *In vivo*, the mouse tolerated the implant very well as can be seen when examining the tissue just prior to explantation as well as the assessment with the cytokine antibody array. IL-10 was significantly higher by 6 weeks and TNF-α levels remained relatively constant. A live/dead assay indicated that the cells that had migrated into the scaffold were viable, while histological analysis showed tissue integration with extracellular matrix formation. In summary, the results of this study indicate that D-PHI (already shown to have the appropriate mechanical properties for graft construction) promoted a wound healing MCs and functional EC growth in co-culture, while eliciting an anti-inflammatory response from cells both *in vitro* and *in vivo*.

8.0 FUTURE OF PROJECT

The overall hypothesis of this project is that the temporal activity of MC in a D-PHI tubular scaffold subjected to biomechanical forces, will regulate functional tissue development of a substitute blood vessel that is smaller than 5 mm in diameter, yielding contractile VSMCs and an anti-thrombotic endothelial lining of the vessels.

The goals of the future work include finalizing the design of a porous tubular scaffold that has sufficient strength to undergo dynamic mechanical loading and facilitate viable and functional tissue development. The profile of serum protein binding to D-PHI and the mechanistic interactions with the anti-inflammatory/pro-wound healing phenotype of MCs on D-PHI must be characterized. It is also necessary to determine the mechanical conditioning protocols that contribute to sustaining a co-culture mixture of functional MCs, VSMCs and EC/endothelial progenitor cells using a pulsatile bioreactor. The final future goal of this study is to examine the graft's *in vivo* function by seeding human MCs/VSMCs and MCs/mesenchymal stem cells in a nude rat abdominal aorta bypass model to assess vasoactivity and blood compatibility.

APPENDIX

Methods for immunoblotting were carried out as described in section 4.0 Materials and Methods using human aortic endothelial cells (HAECs). Since it appeared that there could be a difference between the co-culture and EC alone, a loading control (GAPDH) was used to re-examine both CD31 and VE-cadherin with quantification a possibility. We wished to load a near maximal volume for each sample in order to ensure a visible signal and repeat each sample analysis 3 times. Using the volume we loaded and the known concentration of protein we were able to normalize GAPDH intensities first to total protein, then calculate the average for each cell culture type, and then using that number to divide the VE-cadherin or CD31 intensity in order to compare the amount of each biomarker in each cell type.

The results shown in Figures A1 and A2 were carried out with human aortic endothelial cells and not HCAEC. Figure A1A shows immunoblotting analysis of CD 31 and GAPDH where we see CD31 present only in the EC and co-cultures. GAPDH varied widely amongst the different cell types and was not always visible in the MC culture on D-PHI. Figure A1B shows immunoblotting analysis of CD31 and GAPDH expression for MCs cultured for 7 days on D-PHI in 50% HAEC releasate EBM-2 media and 50% RPMI. As can be seen, no CD31 band is observed.

Figure A2 shows the results of immunoblotting analysis for VE-cadherin which we see present in the EC culture as well as the co-culture on both material surfaces. MCs did not express VE-cadherin and there was no significant difference between EC and the co-culture.

Since this experiment was conducted on two different cell types (HCAECs and HAECs) the data could not be combined as it has been shown that there are phenotypic differences in cells from different areas of the vascular tree [96]. However, qualitatively both EC sources expressed CD31.

Figure A2 shows immunoblotting analysis for VE-cadherin on both D-PHI and TCPS. When performing immunoblotting analysis on two different cell types, one which replicates and one which does not, it is difficult to obtain an adequate loading control that can be applied to each cell type, but especially to the co-culture. Levels of GAPDH varied amongst the different cultures as did protein and an attempt to normalize the data to GAPDH that had been normalized to protein did not yield significant quantitative results. No VE-cadherin was expressed from the MCs nor was it possible to observe any significant difference between the co-culture and EC alone. VE-cadherin is an endothelial specific adhesion molecule which is located between junctions of endothelial cells and is of significant importance for maintaining and controlling these contacts [97]. The fact that it is present in the cells on D-PHI further demonstrates this material's potential for vascular graft synthesis. Although not significantly lower, the co-culture demonstrated a trend towards less VE-cadherin being present which may be expected as it has been shown that MCs induce focal loss in the staining of VE-cadherin during transendothelial migration, a process related to the transient and focal disruption of the VE-cadherin complex which occurs during leukocyte transmigration [98].

Figure A1: Immunoblotting analysis of CD31 expression in EC, MC and the co-culture using human aortic endothelial cells on D-PHI and TCPS. Immunoblotting analysis was performed on cell lysates using an antibody to CD31 after 7 days in culture on D-PHI and TCPS; sample immunoblot (A). GAPDH analysis was performed on the same gel as CD31. Immunoblotting analysis of CD31 and GAPDH expression for MCs cultured 7 days on D-PHI in 50% HAEC releasates and 50% RPMI; sample immunoblot (B). Protein bands were visualized with an enhanced chemiluminescence detection system (Thermo Scientific, SuperSignal West Pico and Femto). S(n=1,2,3) are obtained from three different donors. (prepared by Kelsey Santerre)

A

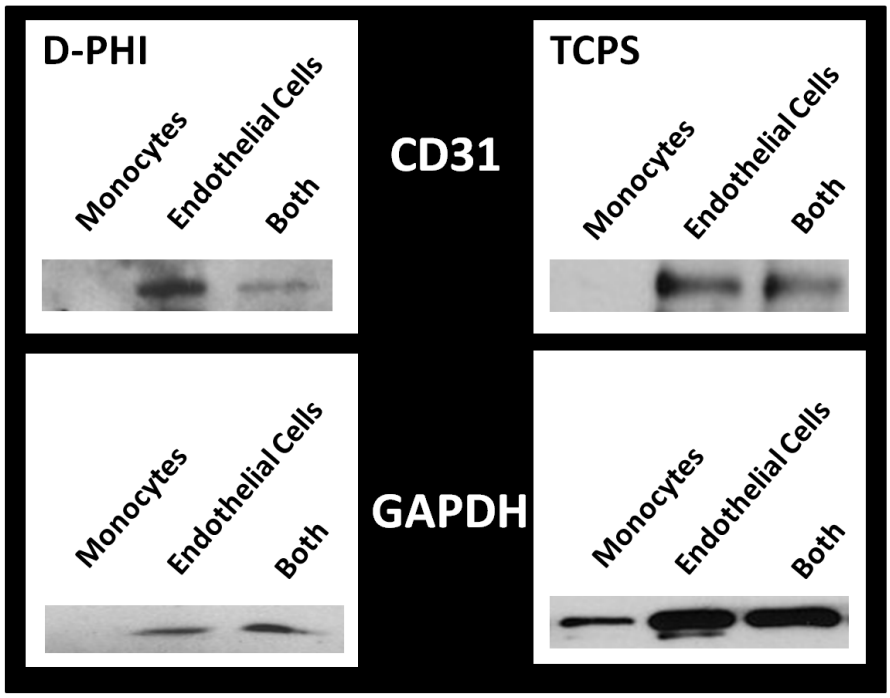
D-PHI
Monocytes
Endothelial Cells
Both
CD31
TCPS
Monocytes
Endothelial Cells
Both
Monocytes
Endothelial Cells
Both
GAPDH
Monocytes
Endothelial Cells
Both

B

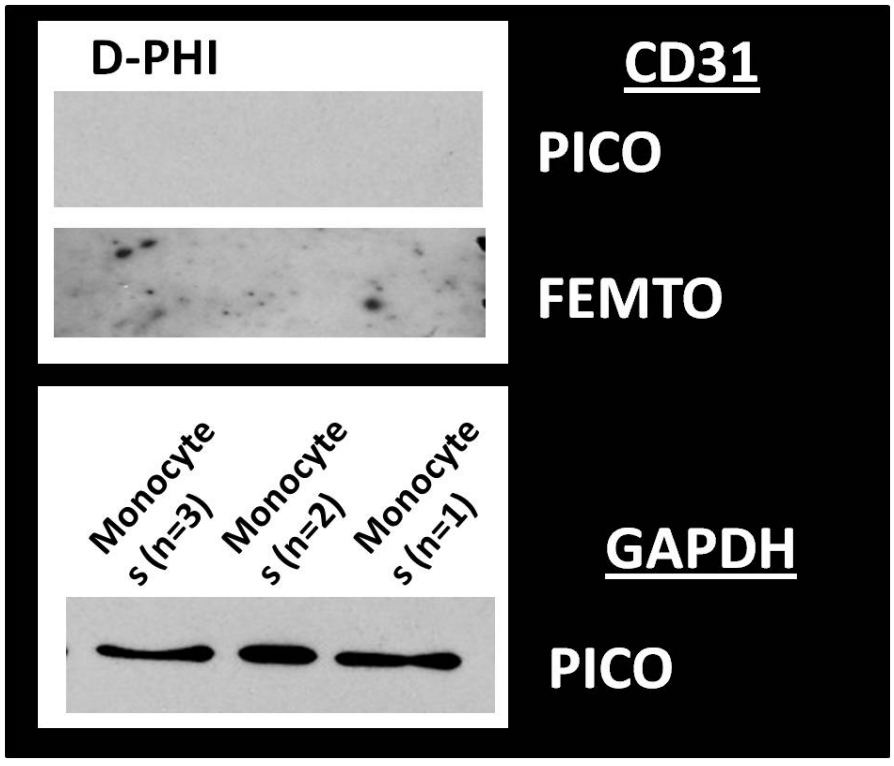
D-PHI
CD31
PICO
FEMTO
Monocyte s (n=3)
Monocyte s (n=2)
Monocyte s (n=1)
GAPDH
PICO

Figure A2: Immunoblotting analysis of VE-cadherin expression in EC, MC and the co-culture using human aortic endothelial cells. Immunoblotting analysis was performed on cell lysates using an antibody to VE Cadherin after 7 days in culture on D-PHI and TCPS; sample immunoblot. GAPDH analysis was performed on the same gel as VE-Cadherin using 1:5000 dilution of GAPDH. Protein bands were visualized with an enhanced chemiluminescence detection system (Thermo Scientific, SuperSignal West Pico and Femto) (prepared by Kelsey Santerre)

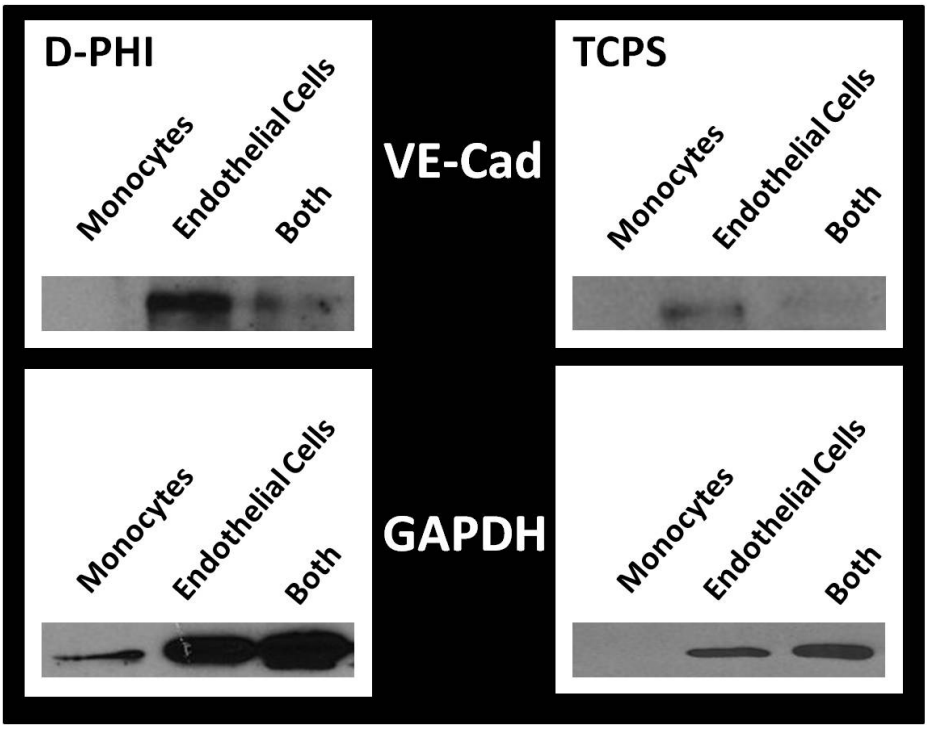
D-PHI
Monocytes
Endothelial Cells
Both
VE-Cad
TCPS
Monocytes
Endothelial Cells
Both
Monocytes
Endothelial Cells
Both
GAPDH
Monocytes
Endothelial Cells
Both

REFERENCES

1. Belch JJ, Topol EJ, Agnelli G, Bertrand M, Califf RM, Clement DL, et al. Critical issues in peripheral arterial disease detection and management: a call to action. Archives of internal medicine 2003;163(8):884-892.
2. Sharifpoor S, Labow RS, Santerre JP. Synthesis and characterization of degradable polar hydrophobic ionic polyurethane scaffolds for vascular tissue engineering applications. Biomacromolecules 2009;10(10):2729-2739.
3. McBane JE, Matheson LA, Sharifpoor S, Santerre JP, Labow RS. Effect of polyurethane chemistry and protein coating on monocyte differentiation towards a wound healing phenotype macrophage. Biomaterials 2009;30(29):5497-5504.
4. Mukherjee D, Cho L. Peripheral arterial disease: considerations in risks, diagnosis, and treatment. Journal of the National Medical Association 2009;101(10):999-1008.
5. O'Loughlin A, McIntosh C, Dinneen SF, O'Brien T. Review paper: basic concepts to novel therapies: a review of the diabetic foot. The international journal of lower extremity wounds;9(2):90-102.
6. Ouriel K. Peripheral arterial disease. Lancet 2001;358(9289):1257-1264.
7. Collaborative meta-analysis of randomised trials of antiplatelet therapy for prevention of death, myocardial infarction, and stroke in high risk patients. BMJ (Clinical research ed 2002;324(7329):71-86.
8. Imparato AM, Kim GE, Davidson T, Crowley JG. Intermittent claudication: its natural course. Surgery 1975;78(6):795-799.
9. Heart Disease and Stroke Statistics -2005 Update. Dallas, Texas: American Heart Association, 2005.
10. Kakisis JD, Liapis CD, Breuer C, Sumpio BE. Artificial blood vessel: the Holy Grail of peripheral vascular surgery. J Vasc Surg 2005;41(2):349-354.
11. Jankowski RJ, Wagner WR. Directions in cardiovascular tissue engineering. Clinics in plastic surgery 1999;26(4):605-616, ix.
12. Zacek M, Konfrst J, Klimes F. Some mechanical/hydrodynamical problems of contemporary vascular grafts. The International journal of artificial organs 1992;15(7):422-425.
13. Nerem RM, Seliktar D. Vascular tissue engineering. Annual review of biomedical engineering 2001;3:225-243.
14. Stegemann JP, Nerem RM. Phenotype modulation in vascular tissue engineering using biochemical and mechanical stimulation. Annals of biomedical engineering 2003;31(4):391-402.
15. Bonfield W. Designing porous scaffolds for tissue engineering. Philosophical transactions 2006;364(1838):227-232.
16. Kim WS, Seo JW, Rho JR, Kim WG. Histopathologic changes of acellularized xenogenic carotid vascular grafts implanted in a pig-to-goat model. The International journal of artificial organs 2007;30(1):44-52.
17. Derham C, Yow H, Ingram J, Fisher J, Ingham E, Korrosis SA, et al. Tissue engineering small-diameter vascular grafts: preparation of a biocompatible porcine ureteric scaffold. Tissue engineering 2008;14(11):1871-1882.

18. Daniel J, Abe K, McFetridge PS. Development of the human umbilical vein scaffold for cardiovascular tissue engineering applications. Asaio J 2005;51(3):252-261.
19. Ketchedjian A, Kreuger P, Lukoff H, Robinson E, Linthurst-Jones A, Crouch K, et al. Ovine panel reactive antibody assay of HLA responsivity to allograft bioengineered vascular scaffolds. The Journal of thoracic and cardiovascular surgery 2005;129(1):159-166.
20. Jay SM, Shepherd BR, Bertram JP, Pober JS, Saltzman WM. Engineering of multifunctional gels integrating highly efficient growth factor delivery with endothelial cell transplantation. Faseb J 2008;22(8):2949-2956.
21. L'Heureux N, Dusserre N, Konig G, Victor B, Keire P, Wight TN, et al. Human tissue-engineered blood vessels for adult arterial revascularization. Nature medicine 2006;12(3):361-365.
22. Konig G, McAllister TN, Dusserre N, Garrido SA, Iyican C, Marini A, et al. Mechanical properties of completely autologous human tissue engineered blood vessels compared to human saphenous vein and mammary artery. Biomaterials 2009;30(8):1542-1550.
23. Zeltinger J, Sherwood JK, Graham DA, Mueller R, Griffith LG. Effect of pore size and void fraction on cellular adhesion, proliferation, and matrix deposition. Tissue Eng 2001;7(5):557-572.
24. Xue L, Greisler HP. Biomaterials in the development and future of vascular grafts. J Vasc Surg 2003;37(2):472-480.
25. Hsu SH, Tseng HJ, Fang ZK. Polyurethane blended with polylactides for improved cell adhesion and reduced platelet activation. Artificial organs 1999;23(10):958-961.
26. Lee SH, Kim BS, Kim SH, Choi SW, Jeong SI, Kwon IK, et al. Elastic biodegradable poly(glycolide-co-caprolactone) scaffold for tissue engineering. Journal of biomedical materials research 2003;66(1):29-37.
27. Li H C, J. pH-compensation effect of bioactive inorganic fillers on the degradation of PLGA. Comp Sci Tech 2005;65:2226-2232.
28. Anderson JM, Rodriguez A, Chang DT. Foreign body reaction to biomaterials. Seminars in immunology 2008;20(2):86-100.
29. Anderson JM. Multinucleated giant cells. Curr Opin Hematol 2000;7(1):40-47.
30. Gretzer C, Emanuelsson L, Liljensten E, Thomsen P. The inflammatory cell influx and cytokines changes during transition from acute inflammation to fibrous repair around implanted materials. Journal of biomaterials science 2006;17(6):669-687.
31. Marchant R, Hiltner A, Hamlin C, Rabinovitch A, Slobodkin R, Anderson JM. In vivo biocompatibility studies. I. The cage implant system and a biodegradable hydrogel. J Biomed Mater Res 1983;17(2):301-325.
32. Anderson JM. Mechanisms of inflammation and infection with implanted devices. Cardiovasc Pathol 1993;4(3):33S-41S.
33. Kao WJ, McNally AK, Hiltner A, Anderson JM. Role for interleukin-4 in foreign-body giant cell formation on a poly(etherurethane urea) in vivo. J Biomed Mater Res 1995;29(10):1267-1275.
34. Bonfield TL, Colton E, Anderson JM. Plasma protein adsorbed biomedical polymers: activation of human monocytes and induction of interleukin 1. J Biomed Mater Res 1989;23(6):535-548.

35. Mosser DM. The many faces of macrophage activation. Journal of leukocyte biology 2003;73(2):209-212.
36. Mantovani A, Sica A, Locati M. New vistas on macrophage differentiation and activation. European journal of immunology 2007;37(1):14-16.
37. Lolmede K, Campana L, Vezzoli M, Bosurgi L, Tonlorenzi R, Clementi E, et al. Inflammatory and alternatively activated human macrophages attract vessel-associated stem cells, relying on separate HMGB1- and MMP-9-dependent pathways. Journal of leukocyte biology 2009;85(5):779-787.
38. Lang I, Schweizer A, Hiden U, Ghaffari-Tabrizi N, Hagendorfer G, Bilban M, et al. Human fetal placental endothelial cells have a mature arterial and a juvenile venous phenotype with adipogenic and osteogenic differentiation potential. Differentiation; research in biological diversity 2008;76(10):1031-1043.
39. Wagner WH, Henderson RM, Hicks HE, Banes AJ, Johnson G, Jr. Differences in morphology, growth rate, and protein synthesis between cultured arterial and venous endothelial cells. J Vasc Surg 1988;8(4):509-519.
40. Vartanian KB, Kirkpatrick SJ, McCarty OJ, Vu TQ, Hanson SR, Hinds MT. Distinct extracellular matrix microenvironments of progenitor and carotid endothelial cells. Journal of biomedical materials research 2009;91(2):528-539.
41. Tepper OM, Galiano RD, Capla JM, Kalka C, Gagne PJ, Jacobowitz GR, et al. Human endothelial progenitor cells from type II diabetics exhibit impaired proliferation, adhesion, and incorporation into vascular structures. Circulation 2002;106(22):2781-2786.
42. Hibbert B, Ma X, Pourdjabbar A, Holm E, Rayner K, Chen YX, et al. Inhibition of endothelial progenitor cell glycogen synthase kinase-3beta results in attenuated neointima formation and enhanced re-endothelialization after arterial injury. Cardiovascular research 2009;83(1):16-23.
43. Gong Z, Niklason LE. Small-diameter human vessel wall engineered from bone marrow-derived mesenchymal stem cells (hMSCs). Faseb J 2008;22(6):1635-1648.
44. Tanaka K, Sata M, Hirata Y, Nagai R. Diverse contribution of bone marrow cells to neointimal hyperplasia after mechanical vascular injuries. Circulation research 2003;93(8):783-790.
45. Vanhoutte PM. Endothelial dysfunction: the first step toward coronary arteriosclerosis. Circ J 2009;73(4):595-601.
46. Cao Y, Poon YF, Feng J, Rayatpisheh S, Chan V, Chan-Park MB. Regulating orientation and phenotype of primary vascular smooth muscle cells by biodegradable films patterned with arrays of microchannels and discontinuous microwalls. Biomaterials;31(24):6228-6238.
47. Wang HQ, Huang LX, Qu MJ, Yan ZQ, Liu B, Shen BR, et al. Shear stress protects against endothelial regulation of vascular smooth muscle cell migration in a coculture system. Endothelium 2006;13(3):171-180.
48. Tran PK, Tran-Lundmark K, Soininen R, Tryggvason K, Thyberg J, Hedin U. Increased intimal hyperplasia and smooth muscle cell proliferation in transgenic mice with heparan sulfate-deficient perlecan. Circulation research 2004;94(4):550-558.
49. Schubert SY, Benarroch A, Ostvang J, Edelman ER. Regulation of endothelial cell proliferation by primary monocytes. Arteriosclerosis, thrombosis, and vascular biology 2008;28(1):97-104.

50. Zilla P, Bezuidenhout D, Human P. Prosthetic vascular grafts: wrong models, wrong questions and no healing. Biomaterials 2007;28(34):5009-5027.
51. Selvin E, Erlinger TP. Prevalence of and risk factors for peripheral arterial disease in the United States: results from the National Health and Nutrition Examination Survey, 1999-2000. Circulation 2004;110(6):738-743.
52. Goodney PP, Beck AW, Nagle J, Welch HG, Zwolak RM. National trends in lower extremity bypass surgery, endovascular interventions, and major amputations. J Vasc Surg 2009;50(1):54-60.
53. Scholz D, Ito W, Fleming I, Deindl E, Sauer A, Wiesnet M, et al. Ultrastructure and molecular histology of rabbit hind-limb collateral artery growth (arteriogenesis). Virchows Arch 2000;436(3):257-270.
54. Voskuil M, van Royen N, Hoefer IE, Seidler R, Guth BD, Bode C, et al. Modulation of collateral artery growth in a porcine hindlimb ligation model using MCP-1. Am J Physiol Heart Circ Physiol 2003;284(4):H1422-1428.
55. Owens GK. Role of mechanical strain in regulation of differentiation of vascular smooth muscle cells. Circulation research 1996;79(5):1054-1055.
56. Owens GK, Kumar MS, Wamhoff BR. Molecular regulation of vascular smooth muscle cell differentiation in development and disease. Physiological reviews 2004;84(3):767-801.
57. Sharifpoor S, Simmons CA, Labow RS, Santerre JP. A study of vascular smooth muscle cell function under cyclic mechanical loading in a polyurethane scaffold with optimized porosity. Acta biomaterialia 2010;6:4218
58. Isenberg BC, Williams C, Tranquillo RT. Small-diameter artificial arteries engineered in vitro. Circulation research 2006;98(1):25-35.
59. Birukov KG, Frid MG, Rogers JD, Shirinsky VP, Koteliansky VE, Campbell JH, et al. Synthesis and expression of smooth muscle phenotype markers in primary culture of rabbit aortic smooth muscle cells: influence of seeding density and media and relation to cell contractility. Experimental cell research 1993;204(1):46-53.
60. Pinchuk L. A review of the biostability and carcinogenicity of polyurethanes in medicine and the new generation of 'biostable' polyurethanes. Journal of biomaterials science 1994;6(3):225-267.
61. Zdrahala RJ, Zdrahala IJ. Biomedical applications of polyurethanes: a review of past promises, present realities, and a vibrant future. Journal of biomaterials applications 1999;14(1):67-90.
62. Labow RS, Sa D, Matheson LA, Santerre JP. Polycarbonate-urethane hard segment chemistry influences esterase substrate specificity for human macrophage mediated biodegradation. Journal of biomaterials science 2005;16:1167-1177.
63. Matheson LA, Santerre JP, Labow RS. Changes in macrophage function and morphology due to biomedical polyurethane surfaces undergoing biodegradation. J Cell Physiol 2004;199(1):8-19.
64. Labow RS, Sa D, Matheson LA, Dinnes DL, Paul Santerre J. The human macrophage response during differentiation and biodegradation on polycarbonate-based polyurethanes: Dependence on hard segment chemistry. Biomaterials 2005;26(35):7357-7366.

65. McBane JE, Ebadi D, Sharifpoor S, Labow RS, Santerre JP. Differentiation of monocytes on a degradable, polar-hydrophobic-ionic polyurethane: 2-dimensional films versus 3-dimensional scaffolds. Acta biomaterialia 2011;7:115-122
66. Joanne E. McBane S, Kuihua Cai, Rosalind S. Labow, and J. Paul Santerre. Influence of co-culturing monocytes with smooth muscle cells: Effects on cell attachment, phenotype, metabolism and migration inot a degradable polyurethane scaffold for vascular tissue regeneration. Abstract TERMIS, Sydney, Australia 2010.
67. McBane JE, Santerre JP, Labow R. Effect of phorbol esters on the macrophage-mediated biodegradation of polyurethanes via protein kinase C activation and other pathways. Journal of biomaterials science 2009;20(4):437-453.
68. McBane JE, Santerre JP, Labow RS. The role of protein kinase C in the monocyte-derived macrophage mediated biodegradation of polycarbonate-based polyurethanes. J Biomed Mater Res 2005;74A:1-11.
69. Bradford MM. A rapid and sensitive method for the quantitation of microgram quantities of protein utilizing the principle of protein-dye binding. Analytical biochemistry 1976;72:248-254.
70. Thevenot P T, L. Novel method to monitor cell survival and distribution in a PLGA degradable scaffold. . 2007;54:39-42.
71. Papadimitriou JM, Ashman RB. Macrophages: current views on their differentiation, structure, and function. Ultrastructural pathology 1989;13(4):343-372.
72. Labow RS, Meek E, Santerre JP. Model systems to assess the destructive potential of human neutrophils and monocyte-derived macrophages during the acute and chronic phases of inflammation. J Biomed Mater Res 2001;54(2):189-197.
73. Labow RS, Meek E, Santerre JP. Hydrolytic degradation of poly(carbonate)-urethanes by monocyte-derived macrophages. Biomaterials 2001;22(22):3025-3033.
74. Uphoff CC, Drexler HG. Biology of monocyte-specific esterase. Leuk Lymphoma 2000;39(3-4):257-270.
75. Joanne E. McBane KC, Loren Matheson, Soroor Sharifpoor, Rosalind S. Labow, and J. Paul Santerre. Testing the in vivo compatibility and biodegradation of a degradable-polar/hydrophobic/ionic polyurethane for vascular tissue engineering applications. Soc for Biomater Ann Mtg, April 21-24, 2010, Seattle, WA
76. Monahan-Earley RA, Isomura T, Garcia RI, Galli SJ, Dvorak HF, Dvorak AM. Nonspecific esterase activity expressed in Weibel-Palade bodies of cloned guinea pig aortic endothelial cells. J Histochem Cytochem 1987;35(5):531-539.
77. Santerre JP, Woodhouse K, Laroche G, Labow RS. Understanding the biodegradation of polyurethanes: From classical implants to tissue engineering materials. Biomaterials 2005;26(35):7457-7470.
78. Labow RS, Meek E, Santerre JP. The biodegradation of poly(urethane)s by the esterolytic activity of serine proteases and oxidative enzyme systems. Journal of biomaterials science 1999;10(7):699-713.
79. Conklin BS, Richter ER, Kreutziger KL, Zhong DS, Chen C. Development and evaluation of a novel decellularized vascular xenograft. Med Eng Phys 2002;24(3):173-183.
80. Dvorin EL, Wylie-Sears J, Kaushal S, Martin DP, Bischoff J. Quantitative evaluation of endothelial progenitors and cardiac valve endothelial cells: proliferation and differentiation on poly-glycolic acid/poly-4-hydroxybutyrate scaffold in response to

vascular endothelial growth factor and transforming growth factor beta1. Tissue Eng 2003;9(3):487-493.
81. Boyer M, Townsend LE, Vogel LM, Falk J, Reitz-Vick D, Trevor KT, et al. Isolation of endothelial cells and their progenitor cells from human peripheral blood. J Vasc Surg 2000;31(1 Pt 1):181-189.
82. Schutte RJ, Parisi-Amon A, Reichert WM. Cytokine profiling using monocytes/macrophages cultured on common biomaterials with a range of surface chemistries. Journal of biomedical materials research 2009;88(1):128-139.
83. Noble KE, Harkness D, Yong KL. Interleukin 10 regulates cellular responses in monocyte/endothelial cell co-cultures. British journal of haematology 2000;108(3):497-504.
84. Mostafa Mtairag E, Chollet-Martin S, Oudghiri M, Laquay N, Jacob MP, Michel JB, et al. Effects of interleukin-10 on monocyte/endothelial cell adhesion and MMP-9/TIMP-1 secretion. Cardiovascular research 2001;49(4):882-890.
85. Christenson EM, Dadsetan M, Wiggins M, Anderson JM, Hiltner A. Poly(carbonate urethane) and poly(ether urethane) biodegradation: in vivo studies. J Biomed Mater Res 2004;69A(3):407-416.
86. Fujimoto K, Inoue H, Ikada Y. Protein adsorption and platelet adhesion onto polyurethane grafted with methoxy-poly(ethylene glycol) methacrylate by plasma technique. J Biomed Mater Res 1993;27(12):1559-1567.
87. Amabile PG, Wong H, Uy M, Boroumand S, Elkins CJ, Yuksel E, et al. In vivo vascular engineering of vein grafts: directed migration of smooth muscle cells by perivascular release of elastase limits neointimal proliferation. J Vasc Interv Radiol 2002;13(7):709-715.
88. Ho LS, He Q, Chen J, Xu P, Tsang LL, Yu S, et al. Interaction between endometrial epithelial cells and blood leukocytes promotes cytokines release and epithelial barrier function in response to Chlamydia trachomatis lipopolysaccharide stimulation. Cell biology international.
89. Esen N, Kielian T. Effects of low dose GM-CSF on microglial inflammatory profiles to diverse pathogen-associated molecular patterns (PAMPs). Journal of neuroinflammation 2007;4:10.
90. Gabay C. Interleukin-6 and chronic inflammation. Arthritis research & therapy 2006;8 Suppl 2:S3.
91. Appay V, Brown A, Cribbes S, Randle E, Czaplewski LG. Aggregation of RANTES is responsible for its inflammatory properties. Characterization of nonaggregating, noninflammatory RANTES mutants. The Journal of biological chemistry 1999;274(39):27505-27512.
92. Aggarwal BB, Shishodia S, Ashikawa K, Bharti AC. The role of TNF and its family members in inflammation and cancer: lessons from gene deletion. Current drug targets 2002;1(4):327-341.
93. Williams-Skipp C, Raman T, Valuck RJ, Watkins H, Palmer BE, Scheinman RI. Unmasking of a protective tumor necrosis factor receptor I-mediated signal in the collagen-induced arthritis model. Arthritis and rheumatism 2009;60(2):408-418.
94. Murray PJ. The primary mechanism of the IL-10-regulated antiinflammatory response is to selectively inhibit transcription. Proceedings of the National Academy of Sciences of the United States of America 2005;102(24):8686-8691.

95. Marie C, Pitton C, Fitting C, Cavaillon JM. Regulation by anti-inflammatory cytokines (IL-4, IL-10, IL-13, TGFbeta)of interleukin-8 production by LPS- and/ or TNFalpha-activated human polymorphonuclear cells. Mediators of inflammation 1996;5(5):334-340.
96. dela Paz NG, D'Amore PA. Arterial versus venous endothelial cells. Cell and tissue research 2009;335(1):5-16.
97. Vestweber D. VE-cadherin: the major endothelial adhesion molecule controlling cellular junctions and blood vessel formation. Arteriosclerosis, thrombosis, and vascular biology 2008;28(2):223-232.
98. Allport JR, Muller WA, Luscinskas FW. Monocytes induce reversible focal changes in vascular endothelial cadherin complex during transendothelial migration under flow. The Journal of cell biology 2000;148(1):203-216.